The Thesis Committee for Karole Lynn Blythe
Certifies that this is the approved version of the following thesis:

Ground state depletion microscopy for imaging the interactions between gold nanoparticles and fluorescent molecules

APPROVED BY
SUPERVISING COMMITTEE:

Supervisor:

Katherine Willets

Jennifer Brodbelt

Ground state depletion microscopy for imaging the interactions between gold nanoparticles and fluorescent molecules

by

Karole Lynn Blythe, BS

Thesis

Presented to the Faculty of the Graduate School of

The University of Texas at Austin

in Partial Fulfillment

of the Requirements

for the Degree of

Master of Arts

The University of Texas at Austin

December 2012

Acknowledgements

I would like to gratefully acknowledge my advisor, Katherine A. Willets, for her support, guidance, and superior MATLAB code writing abilities. I would also like to acknowledge the Willets research group, past and present members, for their support, research ideas, and thoughtful conversations. I would like to especially thank Kathryn M. Mayer, for her tutelage in the areas of MATLAB code writing, microscopy, plasmonics, and nanoparticle synthesis. I would also like to thank my family and friends for their continuous support and encouraging words.

Abstract

Ground state depletion microscopy for imaging the interactions between gold nanoparticles and fluorescent molecules

Karole Lynn Blythe, MA

The University of Texas at Austin, 2012

Supervisor: Katherine Willets

Ground state depletion with individual molecule return (GSDIM) super-resolution microscopy is used to interrogate the location of individual fluorescence bursts from two different nanoparticle-fluorophore systems. The first system consists of fluorophore-labeled DNA molecules on gold nanowire surfaces. In this system carboxytetramethyl rhodamine-labeled double-stranded DNA molecules were bound to the surface of gold nanowires via gold-thiol linkages. The second system focuses on mesoporous silica coated nanorods with dye embedded into the silica coating. The dye molecule, Rhodamine 6G, was incorporated into the silica shell during the nanorod coating procedure. Individual fluorescence bursts were spatially localized using point spread function fitting and used to reconstruct the image of the underlying nanowire or nanorod.

Table of Contents

List of Figures

Chapter 1: *Introduction*

K.L. Blythe et al. *Phys. Chem. Chem. Phys.*, 2012, Advance Article, DOI: 10.1039/C2CP43152A- reproduced by permission of the PCCP Owner Societies.

Gold nanoparticles have become an increasingly popular topic of investigation in the areas of bioimaging[1-4], drug delivery[3-7], and photothermal therapy[1, 4, 8, 9] due to their favorable optical properties (strong scattering, high refractive index sensitivity, and enhanced local electric fields) coupled with their biocompatibility. In most biomedical applications of gold nanoparticles, ligands ranging from antibodies to small drug molecules are attached to nanoparticle surfaces to endow particles with a range of new functions.[5-7, 9] Gold nanoparticles can also be coated with silica to enhance biocompatibility[10-12]. Through silica surface chemistry the silica coated nanoparticle can easily be functionalized with different ligands[13, 14]. Moreover, if the silica shell is porous, fluorescent probes can be embedded into the silica shell[12, 15]. Fluorescent labels are often added, either to provide a secondary optical readout in addition to light scattering or to confirm ligand binding on the nanoparticle surface[16-18]. One challenge with this system is that the fluorescence may couple to plasmon modes of the underlying nanoparticle substrate, and it is challenging to characterize these interactions when multiple fluorophores are near the nanoparticle surface. This is due to the optical diffraction limit, which prevents objects smaller than roughly half the wavelength of light from being resolved.

Recently, super-resolution optical imaging has emerged as a technique for overcoming the diffraction limit of light and resolving images on the ~1 nm length scale, offering us a unique tool for studying the interaction between fluorophore labels and

plasmonic nanostructures. Super-resolution imaging builds on two basic principles: (1) super-localization microscopy, which allows the position of an emitting species to be determined with a precision better than ~5 nm, and (2) active control of the emission state of a fluorescent species, which allows individual emitters to be localized, one at a time[19-22]. Unfortunately, super-resolution imaging techniques based on these two principles are known under a vast array of names, including photoactivated localization microscopy (PALM)[23], stochastic optical reconstruction microscopy (STORM)[19], ground state depletion with individual molecule return (GSDIM)[24] and others[25]. Efforts by the single-molecule imaging community to converge on a single acronym have not yet generated success; in this thesis GSDIM will be favored because the mechanism used for actively controlling the emission properties of the fluorophore is based on ground state depletion, as described below.

For the super-localization component of super-resolution imaging, the diffraction-limited image of a fluorescing dye is fit to a model that describes the point spread function (PSF) of the microscope. The simplest model is to approximate the PSF as a two-dimensional Gaussian function (Equation 1):

$$I = z_0 + I_0 \exp\left[-\frac{1}{2}\left[\left(\frac{x-x_0}{s_x}\right)^2+\left(\frac{y-y_0}{s_y}\right)^2\right]\right]$$

Equation 1

In this equation, I is the spatially-dependent intensity of the diffraction-limited spot, z_0 is the background intensity, I_0 is the peak intensity, x_0 and y_0 are the coordinates of the peak intensity (*i.e.* the centroid position), and s_x and s_y describe the *x* and *y* widths of the peak.

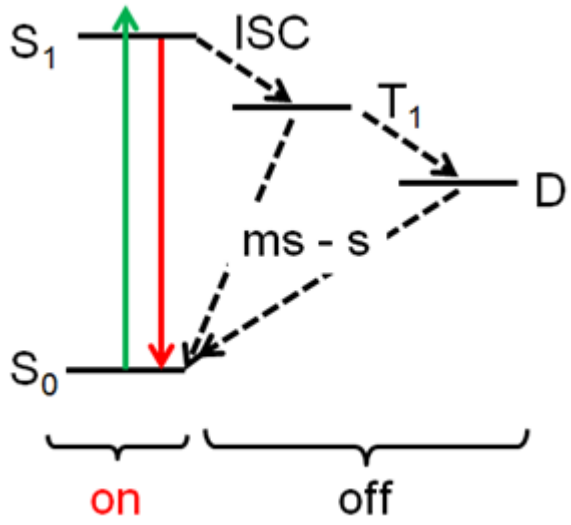

Figure 1.1: Jablonski diagram showing how the ground state depletion process works. A fluorophore is excited from the electronic ground state (S_0) to the first electronic excited state (S_1) and emits a fluorescent photon with a probability given by the fluorescence quantum yield. This is the "on" state of the molecule. Eventually, the molecule will inter-system cross (ISC) into the triplet state (T_1) from where it can also enter metastable dark states (D). This represents the "off" state of the molecule. By controlling the excitation intensity, we can control the number of molecules that are shelved in the off state.

For active control over the emission state of the fluorophore, we exploit the inherent photophyics of a fluorescent dye, Figure 1.1. When a fluorophore is irradiated at the excitation wavelength, it will fluoresce with a probability given by its fluorescence quantum yield; we consider this the "on" state of the molecule. However, there is a small probability that the dye will undergo intersystem crossing, placing the molecule into a nonfluorescent triplet (dark or "off") state, from where it may undergo further transformations to a metastable dark state[24]. Although the rate of intersystem crossing is low, the triplet state lifetime is relatively long (~μs – s) compared to the single molecule

fluorescence lifetime (~ps – ns). Therefore, if an ensemble of dyes is irradiated under sufficiently high laser intensity, after a short time elapses, the vast majority of the dyes will be "shelved" in the dark state. Random dyes will then individually relax back to the ground state, where they will fluoresce until being "re-shelved" into the dark state. It is this stochastic process of molecules switching between the on and off states, creating bursts of fluorescence signal, that allows the position of individual molecules to be localized. By carefully controlling excitation intensity, we can work in the regime where 1-2 dye molecules are in the "on" state at a time, allowing us to track the position of individual fluorophores. For each individual emitter, the centroid coordinates, x_0 and y_0, are obtained from the fit and placed on a scatter plot. By repeating the process over many cycles, we obtain a reconstructed image of the sample, with a resolution much better than the diffraction limit. There are several examples in the literature that use triplet state shelving as a means of modulating fluorescence emission between on and off states in order to achieve super resolution images;[26, 27] as mentioned above, we will use the acronym GSDIM to describe this process.

Super-resolution microscopy has primarily been used in biology to image static structures within cells, such as the cytoskeleton, as well as to track dynamic motions of labeled proteins within the intracellular environment.[28-34] In these systems, the fluorescence is correlated with the exact position of the fluorophore label. However, when studying emitters near plasmonic nanostructures, one must consider that the emission may couple into the plasmon modes of the nanoparticle, which may impact the localization accuracy with respect to the exact position of the molecule. The Willets lab has previously studied this molecule-plasmon coupling extensively using super-resolution imaging of SERS-active nanoclusters [35-38]. The studies described in this thesis will provide insight to whether plasmonic coupling of fluorescence affects the ability to image

individual fluorophores close to the surface of gold nanoparticles and whether that limits the capability of mapping the structure of underlying nanostructures with sub-diffraction resolution.

There are several demonstrations in the literature of super-resolution imaging of fluorophore-coupled plasmonic systems and metal nanoparticles[39-42]. For example, super-resolution imaging of hot spots in aluminum thin films and silver nanoparticle clusters was carried out based on the surface-enhanced fluorescence signal originating from dye molecules in solution around the particle[39]. Super-resolution imaging studies of catalytic reactions at gold nanoparticle surfaces have also been reported, based upon the conversion of Amplex Red to fluorescent resorufin [40]. Davies *et al.* localized stochastic photoblinking from small silver clusters on silver nanowires and observed cooperative emission due to plasmon coupling through the nanowire[41]. Lin *et al.* used super-resolution imaging to image a photoactivated green fluorescent protein variant, Dronpa, on the surface of silver nanowires and arrays of triangular nanoparticles[42]. In all of these examples, the fluorescence was localized with resolution better than 5 nm, yielding insight into electromagnetic hot spots[39], sites of enhanced catalytic activity[40], or the structure of the underlying nanoparticle[40].

In this thesis GSDIM will be used to image the interactions between gold nanoparticles and fluorophores in two different systems: fluorophores attached to gold nanowires with DNA ligands and fluorophores embedded in silica shells around gold nanorod cores. Chapter two includes experimental details on synthesizing the gold nanowires, hybridizing DNA to create the carboxytetramethyl rhodamine-labeled DNA, and finally binding labeled DNA to the gold nanowire. The specific microscopy set up, data analysis, and reconstructed GSDIM results for this system are also discussed in chapter two. Chapter three contains experimental details on synthesizing the mesoporous

silica coated nanorods and how the Rhodamine 6G gets embedded into the pores. The microscopy set up, data analysis, and GSDIM results for the system are also included in chapter three.

Chapter 2: *GSDIM microscopy of gold nanowires and fluorophore-labeled ligands*

K.L. Blythe et al. *Phys. Chem. Chem. Phys.*, 2012, Advance Article, DOI: 10.1039/C2CP43152A- reproduced by permission of the PCCP Owner Societies.

2.1 INTRODUCTION

In this chapter, GSDIM will be used to measure the locations of fluorescent bursts associated with ligands bound on chemically synthesized gold nanowires.[24] These nanoparticles were chosen because they are diffraction-limited in two dimensions, width and height, but have one extended dimension, length, that allows verification on the ability of plasmon-coupled GSDIM to provide sub-diffraction limited resolution. For this study, carboxytetramethyl rhodamine, TAMRA, is used as the fluorophore, since it has been shown to undergo the triplet state shelving process efficiently[43] and is resonant with our excitation laser at 532 nm.

The nanowires are functionalized with double-stranded DNA, with a thiol on one end for binding to the nanowire surface and a TAMRA probe on the other end for fluorescence imaging. The TAMRA has a 6 carbon linker, which should allow sufficient conformational flexibility to negate effects of excitation polarization. In the current study, the dye is chosen such that its excitation (559 nm) and emission (583 nm) wavelengths are far from localized surface plasmon resonances of the nanowires, which are expected to be in the infrared region of the spectrum due to extended length of the nanowires[44]. However, nanowires are well-known to support propagating surface plasmons (or surface plasmon polaritons, SPPs), and the emission may couple into these propagating SPP modes[45-47]. In the studies cited above, a single emitter is positioned near a nanowire to study this coupling; however, it is also possible to study multiple emitters bound along

the length of the nanowire by exploiting the ability to photoswitch each molecule via triplet state shelving, as described in Chapter 1.

2.2 METHODS

2.2.1 Gold nanowire synthesis

Gold nanowires were synthesized according to the method of Huang *et al.*[48] First, a gold seed solution was prepared. Solution 1 was prepared by mixing 19.8 mL of 2.5×10^{-4} M chloroauric acid ($HAuCl_4$) and 0.2 mL of 0.025 M sodium citrate. Solution 2 was prepared by adding 3.783 mg of sodium borohydride into 10 mL of ice-cold 0.025 M sodium citrate solution. The final seed solution was made by mixing 0.6 mL of solution 2 into the entire solution 1; the resulting solution immediately turned red. Next, a growth solution was prepared. First, 25 mL of 0.2 M cetyltrimethylammonium bromide (CTAB) solution was added to 23.75 mL nanopure water. Then, 1.25 mL of 0.01 M $HAuCl_4$ solution was added, resulting in a yellow-orange solution. Next, solutions A, B, and C were prepared from the growth solution. For solution A, 12.5 μL of 0.1 M ascorbic acid solution was added to 2.25 mL of growth solution. Solution B was prepared identically to solution A. For solution C, 125 μL of 0.1 M ascorbic acid solution and 100 μL of concentrated nitric acid were added into 22.5 mL of growth solution. Solutions A, B, and C all turned clear upon the addition of ascorbic acid. Then, the solutions were mixed in the following sequence: 200 μL of the gold seed solution was added into solution A and swirled for 3 s. Then, 200 μL of solution A was added into solution B and swirled for 5 s. Next, 200 μL of solution B was added into solution C. Finally, solution C was allowed to sit overnight at room temperature. The synthesis came to completion over ~12 hours, during this duration the nanowires settled to the bottom of the glass sample container. When the synthesis was completed the supernatant was decanted and the

nanowires were resuspended in 5 mL of nanopure water resulting in an iridescent pinkish- orange solution The nanowires are 1.9 ± 0.3 nm in length and 68.6 ± 12.2 nm in diameter determined from electron micrographs taken using a Hitachi S-5500 STEM.

2.2.2 TAMRA-DNA functionalization of gold nanowires

The gold nanowires were functionalized with double-stranded DNA, of which one end was modified with a thiol group, and the other end carried a TAMRA dye label. The salt aging/salt loading procedure developed by Mirkin co-workers (originally for nanospheres, and later modified for anisotropic particles including nanorods) was used[49]. The DNA was purchased from Integrated DNA Technology as two single-stranded oligos. The first, referred to here as thiol-ssDNA, was modified with a dithiol-containing group at the 3' end and had the following sequence. (thiol-ssDNA: 5' - AAG AAT TTA TAA GCA GAA AAA AAA AAA A [dithiol] - 3') The second, referred to here as TAMRA-ssDNA, was modified with a TAMRA label at its 3' end and had the exact complementary sequence to thiol-ssDNA. The DNA was prepared as follows. First, DNA hybridization was carried out by combining 50 μL each of thiol-ssDNA and TAMRA-ssDNA, both 100 μM in water, in an Eppendorf tube. The resulting solution was placed in a hot water bath at 95° C for 2 minutes. The solution was then removed to room temperature and allowed to sit for 1 hour. Then, 1.54 mg of dithiothreitol (DTT) was added to the solution (for a concentration of 100 mM) in order to cleave the dithiol bond of the thiol-ssDNA. The solution was allowed to sit for 30 minutes. During this time, 200 μL of as-synthesized gold nanowire solution was centrifuged at 10,000 RPM for 20 minutes, decanted, and resuspended in 100 μL of water. The nanowire solution was centrifuged and decanted once more, and the pellet was set aside. The DNA solution was then desalted to remove salt by-products created during the dithiol bond breaking

step using Centri-Spin 20 columns according to the manufacturer's directions. Immediately after desalting, the 100 μL DNA solution was used to resuspend the pellet of nanowires. The resulting solution was allowed to sit for 1 hour. Then, salt aging of the DNA-coated nanowires was carried out as follows. 1 μL 1% sodium dodecyl sulfate (SDS) solution and 10 μL 0.1 M phosphate buffer (pH 7) were added to the nanowire solution to reach concentrations of 0.01% SDS and 0.01 M phosphate buffer. The solution was allowed to sit for 30 minutes. 6 μL 1 M sodium chloride (NaCl) solution was added to the nanowire solution to reach a concentration of 0.05 M NaCl. The solution was allowed to sit for 30 minutes and was then sonicated for ~10 seconds. The same sequence of steps was repeated for five more additions of 1 M NaCl solution in the following volumes (resulting NaCl concentrations in parentheses): 6 μL (0.1 M), 12 μL (0.2 M), 14 μL (0.3 M), 15 μL (0.4 M), 15 μL (0.5 M). Then, the solution was allowed to sit overnight at room temperature. Next, the solution was centrifuged at 10,000 RPM for 20 minutes, decanted, and resuspended in 100 μL of 0.01% SDS solution. Finally, this centrifugation procedure was repeated for two more rounds. Figure 2.1 shows a schematic of the DNA hybridization and the procedure for functionalizing the gold nanowires with the fluorophore-labeled DNA.

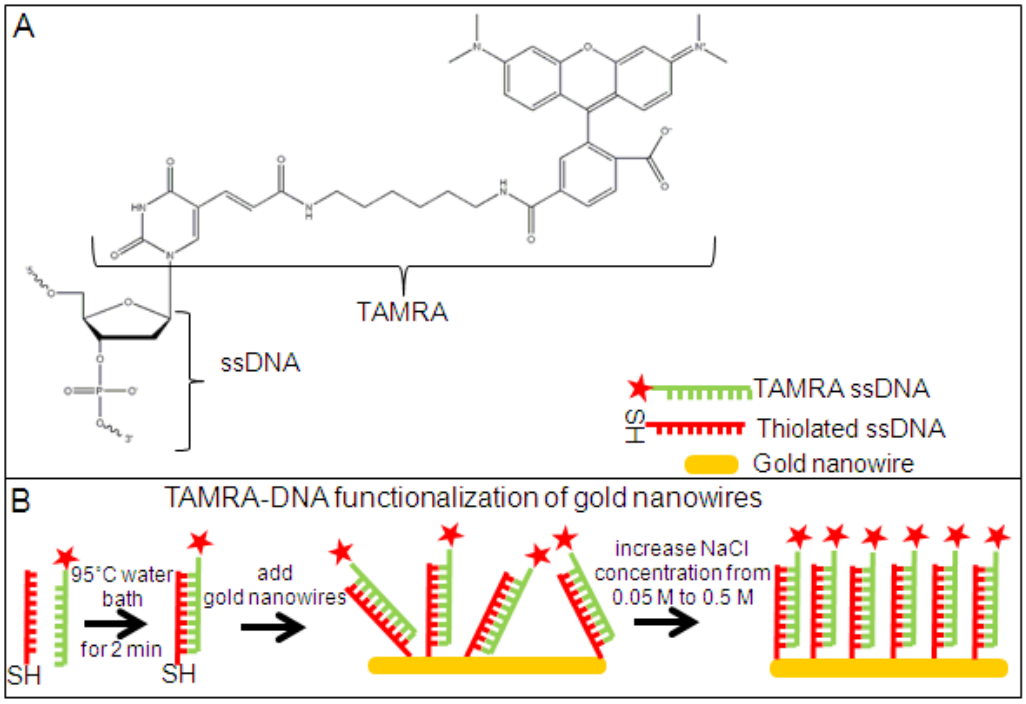

Figure 2.1: (A) The structure of a TAMRA dye molecule attached to the 3' end of a DNA strand provided by the Integrated DNA technologies, Inc website[50]. (B) Illustration of the procedure for functionalizing gold nanowires with fluorophore-labeled DNA.

2.2.3 Sample preparation

25 x 25 mm glass cover slips were washed in piranha solution, 3:1 H_2SO_4:H_2O_2. The cover slips were then rinsed under nanopure water and dried under nitrogen. 5 µL of the above-described functionalized nanowire solution was mixed with 5 µL of a 1:50 dilution (in water) of 0.5 µm SkyBlue fluorescent polystyrene spheres (Spherotech) to be used as alignment markers.[35] The resulting mixture was dropped onto a cover slip and allowed to sit for 5 minutes, followed by rinsing the cover slip with 500-1000 mL of nanopure water by holding the sample under a gentle stream of the water, and then drying under nitrogen.

2.2.4 Microscopy

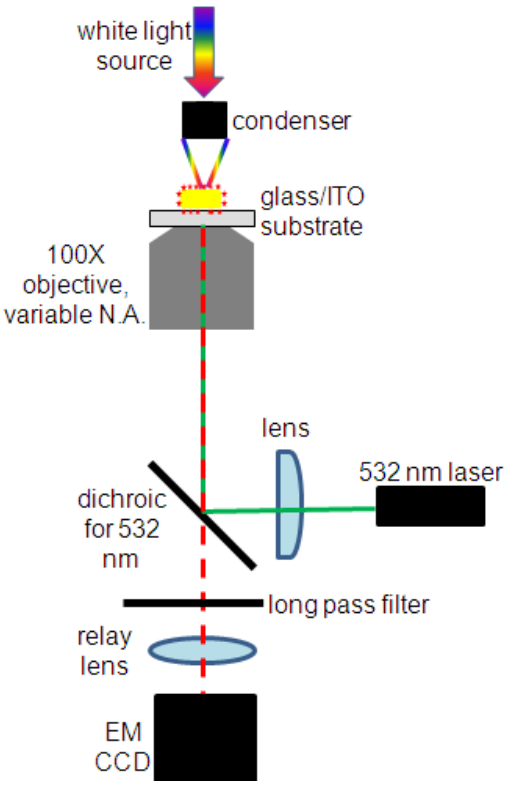

Figure 2.2: Schematic of the optical setup used to collect GSDIM fluorescence emission and dark field images for the nanowire-fluorophore system.

All experiments were carried out on an Olympus IX-71 inverted microscope with an Olympus 100x oil-immersion objective with N.A. variable between 0.6 and 1.3, Figure 2.2. Fluorescence excitation was provided by a 50 mW 532 nm CrystaLaser laser, which was passed through a quarter wave plate to produce quasi-circularly polarized light. The excitation light was passed through a lens before entering the microscope to produce a wide field spot at the sample with a diameter of 5.2 μm. An epi-illumination geometry was used, such that the light was reflected off a 532 dichroic (Semrock Di02-R532-25x36) before entering the objective to illuminate the sample. The resulting fluorescence was collected by the same objective, passed through the 532 nm dichroic

and a long pass filter (Semrock LP03- 532RU) before imaging with an electron-multiplied CCD. Imaging was done via a Princeton Instruments PhotonMax CCD camera. The exposure time for fluorescence imaging was 34.2 ms and the CCD was cleaned pre-exposure. Pre- exposure cleaning was chosen so that the exposure time will equal the camera's readout time, therefore, with the use of an oscilloscope, the exact integration time can be determined. The microscope was also equipped for dark field scattering imaging with a halogen lamp and dark field condenser (Olympus U-DCD 2038101). Dark field scattering images were acquired for 0.3 s. The sample on the stage was covered with a home-built nitrogen flow chamber.

2.2.5 GSDIM data analysis

The raw data consisted of 1875 stacked tiff images of 512 x 512 pixels. Due to timing errors, the first frame is discarded. All analysis was carried out with MATLAB code developed in-house[51]. The procedure can be briefly described as follows: first, the constant nanowire luminescence is removed by subtracting successive frames.[42, 52, 53] Next frames corresponding to fluorescence activity are identified by looking for signals above a pre-determined threshold (3 times the standard deviation of the background). Then each frame is fit to a 2-D Gaussian (equation 1) to extract the centroid position. A 2-D Gaussian is an imperfect model of fluorescence emission near a metal surface, as discussed in detail in Lin et al[42]. However, only Gaussian fits with s_x and s_y widths that fall between a certain range of values and are within 80% of each other are accepted in order to reject PSFs that are distorted by the nearby metal. Finally the centroid data is

plotted create a scatter plot, or the data is binned to create relative frequency and intensity spatial histograms.

2.3 RESULTS AND DISCUSSION

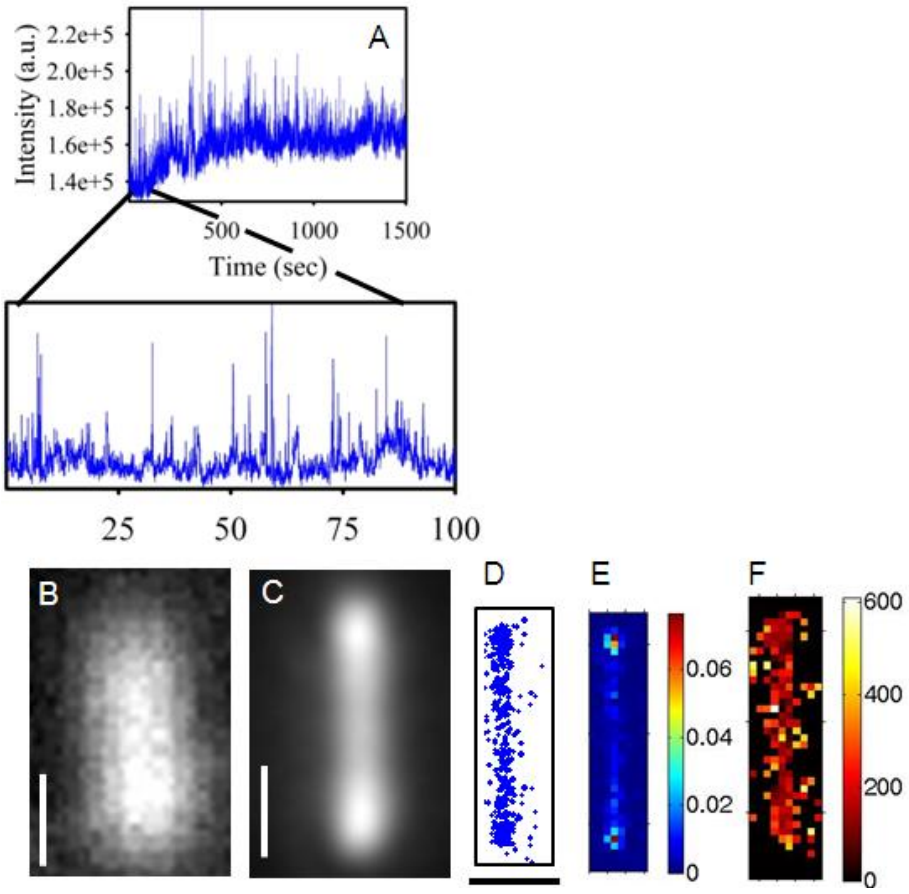

Figure 2.3: (A) Integrated intensity time trace showing fluorescence bursts associated with GSDIM. Inset shows the first 100 seconds of the time trace. (B) Dark field image and (C) summed fluorescence image of the labeled nanowire. (D) Scatter plot showing the values of (x_0, y_0) for the Gaussian fits to each fluorescence burst. (E) Relative frequency histogram showing the percentage of bursts observed at a particular location on the nanowire surface. Bin size is 40 nm. (F) Spatial intensity map showing the average intensity associated with each fluorescent burst on the nanowire surface. Bin size is 40 nm. All images (B-F) have a common 500 nm scale bar.

Figure 2.3 depicts an example of a nanowire labeled with TAMRA-tagged double stranded DNA on its surface. Stoermer and Keating provided evidence that the quenching regime for a fluorophore near a metal surface is less than ~4.8 nm. [54] At 0.34 nm/base pair, the 28 base pair DNA strand used in this study creates a distance of ~9.52 nm between the TAMRA fluorophore and the metal surface; therefore, quenching should not be a major issue. To illustrate the photoswitching typical of GSDIM, an intensity time trace showing the integrated fluorescence intensity as a function of time is shown in Figure 2.3A. This time trace is constructed from 25 individual movies (each of which has up to 1874 frames) and shows that the dynamics persist over many imaging cycles. A zoomed-in insert of the plot is included to emphasize molecules stochastically switching between on and off states. A steadily rising background is observed during the first few movies, which eventually settles with time; it is unclear whether this changing background is due to changes in the inherent luminescence of the gold nanowire[52, 53, 55] or due to weakly emitting TAMRA dyes.

Throughout the time trace, Figure 2.3A, we observe strong fluorescence bursts above the background, which occur when a TAMRA molecule returns from the dark state to the ground state and is able to fluoresce again. It can be stated with confidence that the bursts in Figure 2.3A are assigned as TAMRA undergoing GSDIM. The evidence for this point is show in Figure 2.4. Looking at the time trace from an unlabeled nanowire (Figure 2.4A), several small bursts can be observed, but with much less frequency than the bursts observed from the labeled nanowire (Figure 2.4B) included for comparison. For the nanowire, only 7 bursts of intensity could be localized for the 120 s of data acquisition,

Figure 2.4C. However, the labeled wire yielded 38 localized bursts for the same time frame, Figure 2.4F. When the unlabeled nanowire is processed using the same procedure described above, we find that most of the spurious intensity bursts do not make it through the first step of our fitting procedure. The bursts observed from an unlabeled nanowire can possibly be attributed to interband transitions or impurities on the nanowire surface. [56-59]

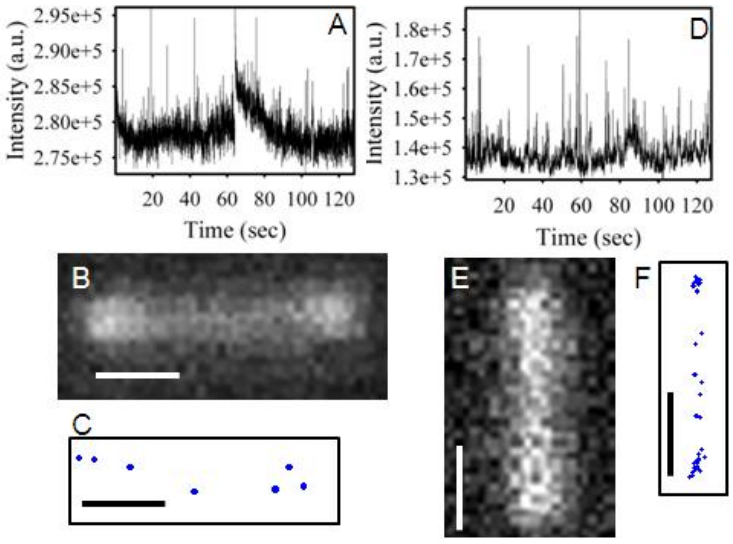

Figure 2.4: (A) Integrated intensity time trace showing bursts associated with gold nanowire luminescence blinking. (B) A single luminescence image of the unlabeled nanowire. (C) Scatter plot showing the values of (x_0, y_0) for the Gaussian fits to each luminescence burst. (D) Integrated intensity time trace showing fluorescence bursts associated with GSDIM. (E) A single fluorescence image of the labeled nanowire. (F) Scatter plot showing the values of (x_0, y_0) for the Gaussian fits to each fluorescent burst. A-C have a common 500 nm scale bar. D-F have a common 500 nm scale bar.

A dark field image of the nanowire is shown in Figure 2.3B and shows that the length of the nanowire is beyond the diffraction limit, as expected. Figure 2.3C shows the sum of 1875 fluorescence images from the first image acquisition, which would mimic the measured fluorescence from multiple simultaneous emitters in the absence of

photoswitching. The nanowire dimensions in this image cannot be determined due to the diffraction limit, nor can anything about possible plasmon-fluorescence coupling be determined.

Next, each individual fluorescent burst is fit to equation 1 to extract its emission centroid; these centroid fits are shown in a scatter plot in Figure 2.3D. The scatter plot creates a reconstructed image of the nanowire. Centroids are located along the entire length of the nanowire, indicating that TAMRA-labeled DNA binds to both the sides and ends of the wire. Next, a 2-D histogram showing the percentage of centroid positions that were localized at a particular location along the nanowire (Figure 2.3E) is created. 40 nm bins were chosen for this histogram, which is more than six times smaller than the diffraction-limited width (here, ~270 nm) and roughly twice the expected width of the nanowire. The frequency histogram is constructed by dividing the number of bursts that occurred in a specific bin by the total number of bursts that happened over the entire experiment. In this experiment, 639 total bursts over 54 movies were measured. On the other hand, it was predicted that ~22,400 TAMRA-labeled DNA molecules would bind to the nanowire, assuming uniform coverage and using a mathematical model published by Hill et al. for single stranded DNA[60]. It should be pointed out that this experiment uses double stranded DNA, which may lead to slightly lower labeling density than predicted; nevertheless, even if the value is off by a factor of ten, only a subset of the fluorophores on the surface is sampled. Given the extended length of the nanowire and the small fraction of observed dyes, smaller histogram bins produce sparse data which is challenging to interpret.

The frequency histogram shows that the highest percentage of GSDIM bursts occurs at the ends of the wire, with two 40x40 nm bins contributing >14% of the total fluorescent bursts in the experiment. There are several possible explanations for this:

first, the preference of biomolecules to bind to the ends of gold nanorods due to steric constraints has been previously hypothesized.[61-63] In particular, the CTAB ligand which is used in the synthesis is known to be more tightly bound on the side facets of nanorods; therefore, ligands can more easily bind at the ends of the rod, where the CTAB bilayer is imperfect.[61, 64-66] If this argument is extended to nanowires, it is expected that a higher number of bound ligands will be present at the nanowire ends, leading to a greater frequency of GSDIM bursts. A second possibility is that the fluorescence is exciting surface plasmon polaritons (SPPs) in the nanowire and the emission is directed down the length of the nanowire, with preferential emission at the nanowire ends.[47, 67-70] This mechanism is consistent with previous reports, in which single emitters in proximity to plasmonic nanowires emit at both the location of the emitter as well as the ends of the nanowire[45-47]. Third, if the electromagnetic field is enhanced at the ends of the nanowire, the increased local intensity could promote enhanced photoswitching and therefore a greater number of GSDIM events.[24, 70-74]

This third hypothesis is the least likely, given the inability to excite localized surface plasmons in the nanowires in the visible region of the spectrum[44]. To further demonstrate this, the average emission intensity was calculated for all centroid points that fall within a given bin in the frequency histogram to create a spatial intensity map (Figure 2.3F).[35] If the ends of the nanowire are associated with enhanced electromagnetic fields, higher average fluorophore intensities at the end of the nanowire would be observed[75]. The resulting spatial intensity map does not show an obvious difference in the intensity of the GSDIM bursts at the ends of the nanowire versus the middle. If electromagnetic enhancement were present, the enhancement in the emission intensity would be orders of magnitude larger at the nanowire ends. Thus, plasmon-mediated electromagnetic field enhancement as an explanation for more fluorescence emission events occurring at the

end of the nanowire is ruled out. However, the present data does not allow either enhanced fluorophore labelling at the nanowires ends or SPP-coupled emission to be ruled out as the responsible mechanism.

If the effective width of the relative frequency histogram and spatial intensity maps shown in Figures 2.3E and 2.3F are compared, it appears that the spatial intensity map in 2.3F is wider. This is an artifact of the calculation, where each intensity bin represents the average intensity for all centroid points within that bin; thus, a single intensity point in a bin will carry equal weight to a bin that contains 40 points. However, the points that lie outside the expected width of the nanowire should not be ignored. It is possible that these points are due to non-specifically bound dyes on the substrate surface; however, one would not expect these to be clustered beside the nanoparticle. Another possibility is that the labeled DNA is being released from the nanowire surface, through either thermal or hot electron processes[76]. This extended width in the spatial intensity map is only observed in this example, where the sample was illuminated for more than 50 individual movies. The remaining examples provided in this chapter are composite images from 3-4 movies, which may explain why this broadening is not seen in the other examples. Nonetheless, it is clear from the relative frequency histogram in Figure 2.3E that the width of the reconstructed nanowire image is less than half the width of the wire in the composite fluorescence image in Figure 2.3C, consistent with the expected nanowire width of ~68 nm.

Figure 2.5 gives two more examples of using GSDIM to map out the structure of individual nanowires and study the spatial origin of the fluorescence emission events. Figures 2.5A and 2.5B shows dark field and composite fluorescence images, respectively, of gold nanowires. In the fluorescence data shown in Figure 2.5B, the fluorescence is more intense at the nanowire ends compared to the center. Because this is a summed

image, this could be due to either brighter gold luminescence occurring at the nanowire ends or a larger fraction of dyes emitting at the nanowire ends. However, by using GSDIM, the fluorescence due to individual TAMRA molecules can be distinguished from the background luminescence of the gold. Using the same histogram analysis as before, ~15% of the GSDIM events occur at the end of the nanowire in this example (Figure 2.4C), but the fluorescence intensity is not orders of magnitude higher at the nanowire ends (Figure 2.5D). Figure 2.5, E-H shows a third nanowire example and the same trends are observed in the two histograms.

Unlike the previous example in Figure 2.5, fluorescence bursts do not appear uniformly along the entire length of the nanowire; there is some patchiness in the frequency histograms in both examples in Figure 2.5. This is most likely due to the fact that fewer frames of data were collected on these nanowires, resulting in incomplete sampling of all ligands on the surface. From before, there are ~22,400 labelled-DNA molecules at full monolayer coverage, yet in the data shown in Figures 2.5C and 2.5G only 116 and 121 bursts, respectively, are observed over the course of the experiment. Even with the limited sampling, the reconstructed images reproduce the expected shape and dimensions of a nanowire extremely well.

One interesting feature of the nanowire shown in Figures 2.5A-D is that it shows a kink in all four images. Kinks in nanowires often behave similar to nanowire ends, given that they are defect sites where light can be coupled into or out of plasmon modes of the nanowire[77]. As such, one might expect to see an increase in the frequency of GSDIM events at the kink in the nanowire, similar to the nanowire ends, if SPPs were the dominant mechanism that led to increased activity at the nanowire ends. Instead, a reduction in the number of GSDIM events was observed close to the nanowire kink. This is consistent with reduced labeling of DNA at that site, possibly due to steric hindrance

on the interior of the kink. It is unlikely that this nanowire is actually two nanowires lying end-to-end because that geometry would create a hot spot between the two nanowires and should lead to increased intensity at that site[78-80].

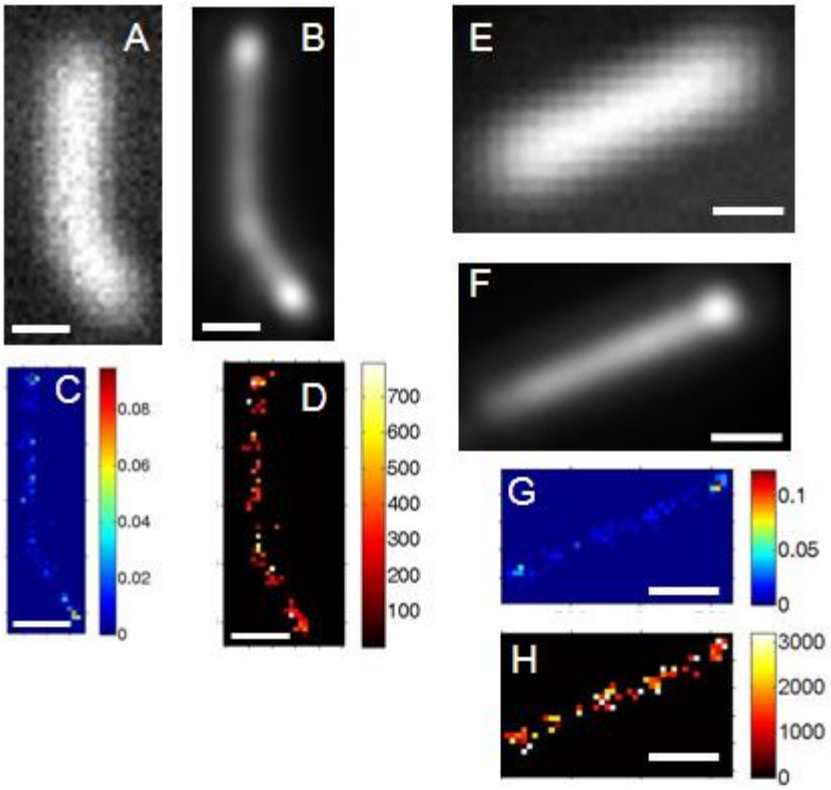

Figure 2.5: (A) Dark field and (B) composite fluorescence image of 1875 summed frames from the first image acquisition of a bent nanowire. (C) Relative frequency histogram and (D) spatial intensity map for the reconstructed nanowire. Bin size is 40 nm. All images (A-D) have a common 500 nm scale bar. (E) Dark field and (F) composite fluorescence image of 1875 summed frames from the first image acquisition of a nanowire. (G) Relative frequency histogram and (H) spatial intensity map for the reconstructed nanowire. Bin size is 40 nm. All images (E-H) have a common 500 nm scale bar.

In the three examples described thus far, the shape of the nanowire was reconstructed from the GSDIM data, yielding nanowire widths of <80 nm, which is

limited only by the bin size of the histograms. In order to compare our reconstructed images with the actual nanostructure of interest, correlated GSDIM and SEM experiments were performed. Indium tin oxide (ITO) slides patterned with an aluminum alpha-numeric grid were used.[37] After the optical data was taken, the slide was attached to a SEM holder using colloidal graphite for electron microscopy.

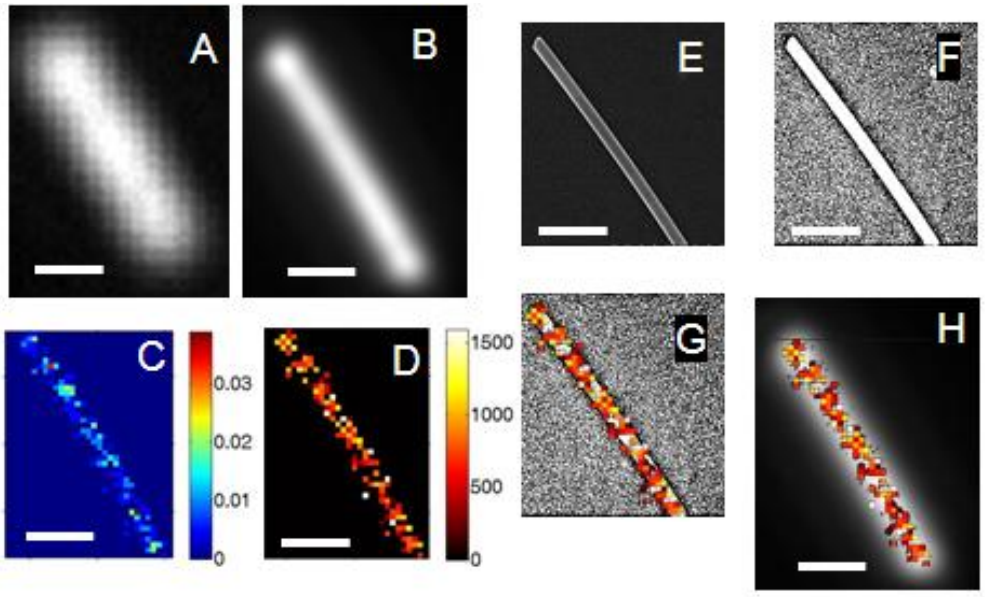

Figure 2.6: (A) Dark field and (B) fluorescence image of a labeled nanowire. (C) Relative frequency histogram and (D) spatial intensity map of the reconstructed nanowire. Bin size is 40 nm. (E) SEM image of the nanowire and (F) re-contrasted SEM image to make the edges of the nanowire more apparent. (G) Intensity histogram overlaid on the SEM image from (F). Note that the width of the reconstructed nanowire agrees with the width from the SEM image. (H) Intensity histogram overlaid on the fluorescence image from (B). Note that the fluorescence image overestimates the width of the nanowire. All images have a common 500 nm scale bar.

Figure 2.6 shows an example of correlated optical and SEM data of the same nanowire. As opposed to the previous examples, in which the highest occurrence of GSDIM events was at the wire ends, the relative frequency histogram in Fig. 2.6C shows

no increase in the number of GSDIM events at the wire ends for this nanowire. However, similarly to the other examples, the spatial intensity map (Figure 2.6D) shows evenly distributed intensity along the nanowire. This result suggests that the DNA is present along the entire length of the nanowire and is consistent with a defect-free nanowire[61, 65, 81]. The accompanying SEM image in Figure 2.6E shows that the edges of the nanowire are smooth, and no obvious small particle defects are present. Figure 2.6G shows the spatial intensity histogram from Figure 2.6D overlaid on the re-contrasted SEM image of the wire (Figure 2.6F). The reconstructed image accurately maps the length and, more importantly, the sub-diffraction limited width of the nanowire, despite the large bin size of the histograms. For comparison, the spatial intensity map was also overlaid on the summed fluorescence image from Figure 2.6B to show how super-resolution imaging provides superior width resolution in contrast to traditional far field imaging.

Figure 2.7 shows a fourth example of a nanowire that shows dramatically different behavior from the previous examples. The dark field image, Figure 2.7A, appears consistent with previous dark field images of nanowires; however, in the summed fluorescence image (Figure 2.7B) the bulk of the emission occurs near the center of the wire. The SEM in Figure 2.7C shows that the site-specific emission is correlated with a spherical nanoparticle attached to the centre of the nanowire. Unlike in previous examples, the GSDIM results converge to a single location, as shown in both the relative frequency histogram (Figure 2.7D) and spatial intensity maps (Figure 2.7E). Although the convergence of the fluorescence to a single region is apparent from the diffraction-limited fluorescence image in Figure 2.7B, the histogram data show that the fluorescence is localized to a single spot much smaller than the diffraction limit. The calculated standard deviation of the frequency histogram and found that the width is ~17 nm, which is smaller than the attached nanoparticle and the diameter of the nanowire.

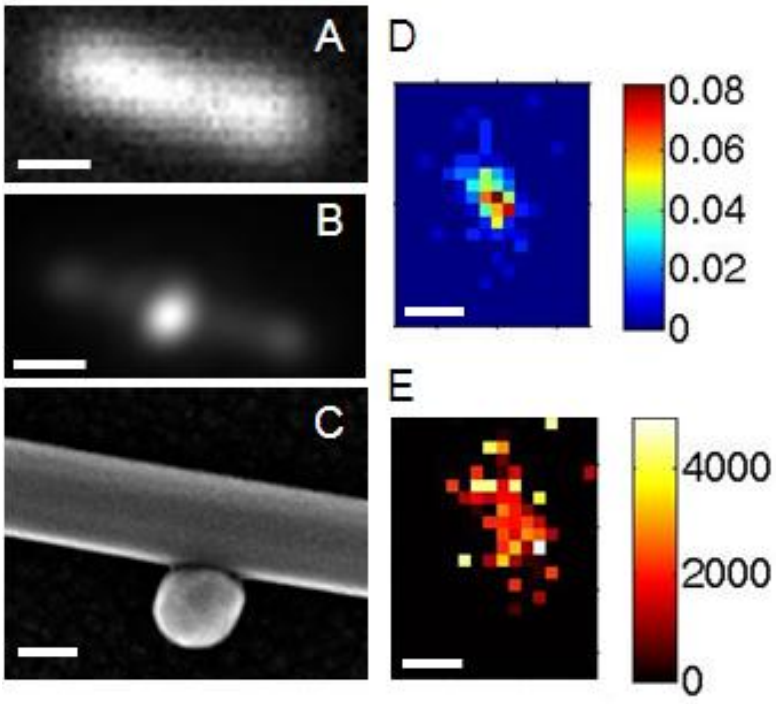

Figure 2.7: (A) Dark field and (B) fluorescence image of a labeled nanowire. The fluorescence image is a sum of 1875 consecutive images from an image stack. (C) SEM image of the nanowire showing a small spherical nanoparticle stuck to its side. (D) Relative frequency histogram and (E) spatial intensity map of the reconstructed image show a single region of GSDIM activity. Bin size is 10 nm. Scale bar is 500 nm for (A-B) and 50 nm for (C-E).

Two possible origins for site-specific emission from the attached nanoparticle can be hypothesized: first, the nanosphere creates a hot spot with the nanowire, leading to a sizable electromagnetic enhancement at the junction.[82, 83] The junction would allow for strong surface-enhanced fluorescence, effectively overwhelming emission from all other dyes.[84] However, the average fluorescence intensity in this example is not orders of magnitude higher than in the other examples. Moreover, one would expect to see some fluorescence events occur at other sites on the nanowire surface, but in this case, the emission is completely localized to a single spot. As a result, the formation of an

electromagnetic “hot spot” does not seem like a plausible explanation for the site-specific emission. A second hypothesis is that the fluorescence from the TAMRA excites SPPs, which propagate down the nanowire and are emitted exclusively at the nanoparticle defect site. Plasmon emission at defect sites is a well-known phenomenon, but it is surprising that in this case all emission occurs at a single site, with no corresponding emission from the nanowire ends.[77, 85] One possibility is that the wavelength of the local plasmon mode at the defect site is better matched in energy to the TAMRA-launched SPP, favoring emission at that site. One fact that supports this hypothesis is that the red-shifted gold luminescence does not couple as efficiently into this single emission site, as evidenced by the dim luminescence spread over the length of the nanowire in Figure 2.7B.

For comparison, Figure 2.8 shows another example of site-specific emission along a nanowire. In this case, the summed fluorescence image (Figure 2.8B) shows two regions of higher overall emission intensity. However, the GSDIM frequency histogram (Figure 2.8C) reveals three dominant emission sites, as well as two less prominent sites in the upper right and lower left. These five localized emission sites are completely obscured by the diffraction-limited emission image in Figure 2.8B, validating the need for super-resolution techniques for exploring these molecule-plasmon interactions. The associated spatial intensity map shows that the intensities of all five emission sites are comparable, similar to the previous results. The SEM image (Figure 2.8E) reveals several small nanoparticles attached to the wire along its length. In Figure 2.8F, the spatial intensity map is overlaid on the SEM image and shows that the three dominant sites of GSDIM emission occur where the attached particles are located, while the two secondary sites are correlated with the nanowire ends. This behavior is consistent with TAMRA-excited SPP modes in the nanowire that emit at defect sites, including the ends of the

nanowire. Because there are several defect sites along the nanowire, multiple regions of site-specific emission are observed.

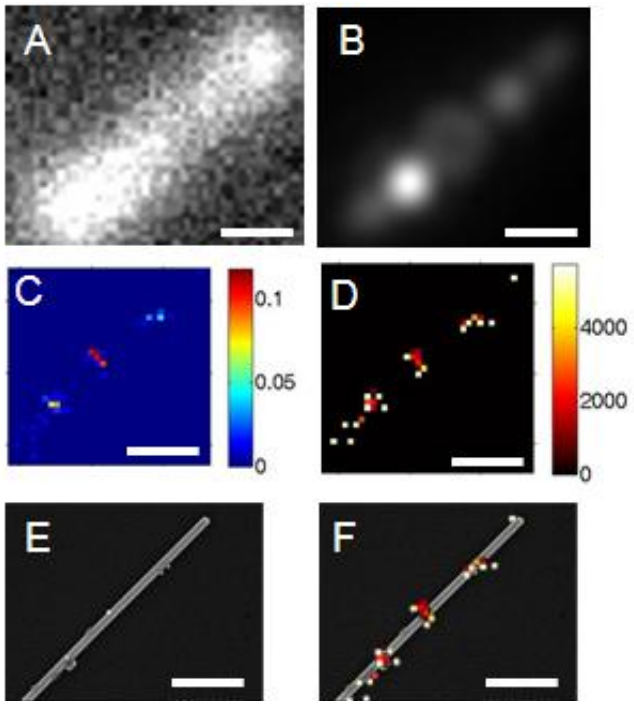

Figure 2.8: (A) Dark field and (B) fluorescence image of a labeled nanowire. The fluorescence image is a sum of 1875 consecutive images from an image stack. (C) Relative frequency histogram and (D) spatial intensity map of the reconstructed image show several confined regions of GSDIM activity. Bin size is 40 nm. (E) SEM image of the nanowire showing several small nanoparticles stuck to its side. (F) Intensity histogram laid on top of the SEM image shows that the regions of GSDIM activity correlate with the location of the attached nanoparticles. All images have a common 500 nm scale bar.

In a final example, shown in Figure 2.9, the nanowire does not have an attached nanoparticle, yet still exhibits site-specific emission. While the fluorescence image (Figure 2.9B) does not show evidence of site-specific emission along the length of the nanowire (in comparison to Figures 2.7B and 2.8B), the histograms from the reconstructed GSDIM images show several regions of isolated GSDIM activity, similar

to Figure 2.8. Unlike the previous two examples, the SEM image (Figure 2.9E) reveals that no nanoparticles are attached to the side of the nanowire (to within the resolution of the SEM). However, the overlaid spatial intensity map and SEM image, shown in Figure 2.9F, shows that GSDIM emission did happen at specific spots on the wire, including the nanowire ends. This behavior could be caused by poor DNA labeling of this specific nanowire or under-sampling of the bound ligands. Alternatively, the nanowire may have small defect sites below the resolution of the SEM, such as gold clusters, which also act as sites for SPP emission. Even though we do not sample fluorescence bursts from molecules along the entire length of the nanowire, we are still able to match its dimensions in both length and width with the reconstructed images.

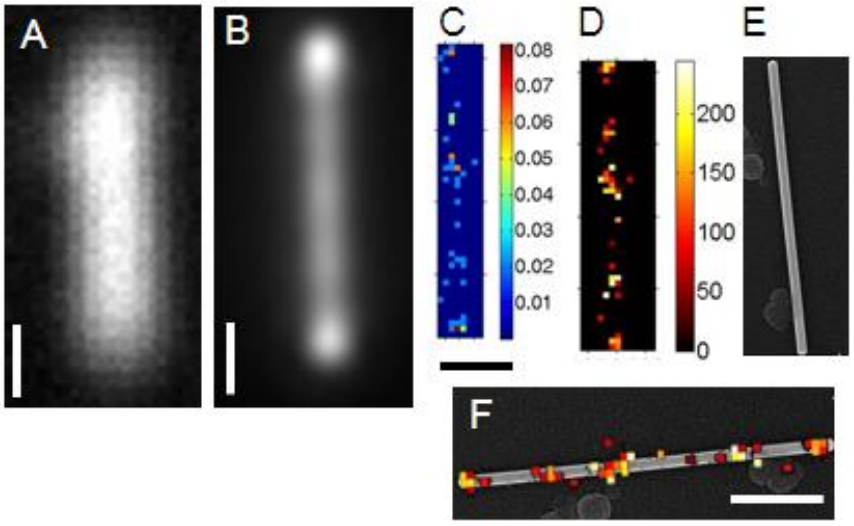

Figure 2.9: (A) Dark field and (B) fluorescence image of a labeled nanowire. The fluorescence image is a sum of 1875 consecutive images from an image stack. (C) Relative frequency histogram and (D) spatial intensity map of the reconstructed image show several confined regions of GSDIM activity. Bin size is 40 nm. (E) SEM image of the isolated and clean nanowire. (F) Intensity histogram laid on top of the SEM image shows that no structural features on the nanowire correspond to the regions of GSDIM emission. Scale bar for image F = 500 nm. Images (A-E) have a common 500 nm scale bar.

Previously, two reasons why emission might be observed at site-specific locations along the length of the nanowire was postulated (a third hypothesis, enhanced electromagnetic fields, was rejected due to lack of evidence for enhanced fluorescence intensity and poor resonance overlap between our excitation/emission and the localized surface plasmon resonance of the nanowire). The first hypothesis was that DNA preferentially labels specific sites along the length of the nanowire, resulting in fluorescence localization at those sites; the second hypothesis was that the fluorescence emission can couple into SPP modes of the nanowire, yielding preferential emission at defect sites along the length of the nanowire. Based on this data, the latter hypothesis does contribute to site-specific emission, as evidenced by the positive correlation between emissive sites and nanoparticle defects on the surface (as in Figure 2.8F). However, contribution of non-uniform DNA labelling on the surface cannot be ruled out. One challenge of studying plasmonic substrates labelled with fluorescent dyes is that the system is strongly coupled, which means that a dye positioned at a particular location may excite a SPP mode, leading to emission many nanometres away from the original fluorescent dye. Link and coworkers have recently imaged SPP propagation lengths of 1.8 μm in nanowires 6.1 μm in length[86]. Thus, the localization accuracy shown here may be many nanometres off, due to this fluorescence-plasmon coupling.

Despite this challenge, this data does reveal that emission can be localized along the entire length of the nanowire and not just at the nanowire ends or defect sites. For example, Figures 2.3, 2.5, and 2.6 show emissions along the entire length of the nanowire, and Figure 2.6 shows that the reconstructed image agrees extremely well with the SEM structural data. Thus, with enough fluorescence emission events, it is possible to reconstruct the underlying shape of the nanowire, even if insight into the ligand density on the surface is lost. In principle, if the length of the DNA spacer is increased, such that

the fluorescence is no longer able to couple into SPP modes of the nanostructure, it will be possible to monitor ligand binding on the surface. By the same argument, decreasing the length of the DNA spacer would promote plasmon-fluorescence coupling, yielding even higher probabilities of site-specific emission. This hypothesis will be explored in future work. It should also be noted that the coupling between molecular fluorescence and SPP modes appears much stronger when small nanoparticles are adjacent to the plasmonic nanowire, serving as defect sites where light can be efficiently out-coupled. Thus, super-resolution imaging provides a unique mechanism for studying the interaction between fluorophore-labeled ligands and plasmonic nanowires, although one must use caution in assigning the location of each fluorescent burst as the actual site of the emitting fluorophore.

2.4 Conclusion

GSDIM is a powerful technique for localizing fluorescence emission from fluorophores bound to the surface of plasmonic nanostructures. Using GSDIM, it is possible to map out the structure of a nanowire, although the location of each fluorescent burst may not correlate to the precise location of the active fluorophore, due to coupling of the fluorescence to SPP modes. Through correlated optical and SEM studies, it can be observed that the reconstructed maps of nanowires provide accurate measurements for both length and width dimensions of the nanowires. The fact that fluorescence emission can couple to SPP modes within the nanowire was also observed. While this phenomenon complicates the analysis of this nanowire-fluorophore system, particularly when small nanoparticles are attached to the nanowire surface, the ability to determine the dimensions of the underlying nanoparticle is maintained. This technique provides a new

approach for studying the complex interaction between plasmonic nanostructures and emitting species, at fluorophore concentrations well above the single molecule level.

2.5 ACKNOWLEDGEMENTS

I gratefully acknowledge Kathryn M. Mayer and Maggie L. Weber for assisting me in the work shown in chapter two. I also acknowledge the NSF IGERT "Atomic and Molecular Imaging" Program (grant no. DGE-0549417) for fellowship support. I would like to thank Spherotech for the generous gift of fluorescent nanospheres used as alignment markers in the nanowire experiments and Kwonnam Sohn of Northwestern University for helpful correspondence regarding the nanowire synthesis. I also thank the National Science Foundation (Grant No. 0821312) for funding the Hitachi S-5500 scanning electron microscope/scanning transmission electron microscope used in this work and Texas Materials Institute for supporting this facility. This material is based on work supported by the Welch Foundation under Award No. F-1699.

Chapter 3: *GSDIM microscopy of dye-doped mesoporous silica coated gold nanorods*

3.1 INTRODUCTION

In this chapter GSDIM will be used to investigate dye molecules embedded into a mesoporous silica shell, which is coating a gold nanorod. The porous silica shell serves the purpose of functionalizing the perimeter of the gold nanorod with fluorophores. It is expected that only the fluorophores embedded into pores on the outer edge of the silica shell will be sampled, thus creating a distance between the gold surface and the fluorophores that is greater than the quenching regime, as discussed briefly in Chapter two. Rhodamine 6G (R6G) will be embedded into pores of the silica coating. R6G was chosen because it is resonant with the 532 nm laser excitation source and because its cationic charge should create a strong ionic bound with the anionic silica surface. It has also been shown that R6G is able to effectively undergo the triplet state shelving process[87, 88]. The expected result for this experiment is reconstructed images of the mesoporous silica coated gold nanorods. The preliminary results for this experiment are included in this chapter.

3.2 METHODS

3.2.1 Gold nanorod synthesis

The gold nanorods were synthesized based on seed mediated growth methods described by Hafner *et al.*[89, 90] and Yan *et al.*[15]. The seed solution was prepared by mixing 0.25 mL of 0.01 M chloroauric acid ($HAuCl_4$) aqueous solution, 9.75 mL of 0.1 M cetyltrimethylammonium bromide (CTAB) aqueous solution, and 0.6 mL of ice cold 0.01 M sodium borohydride aqueous solution together in a scintillation vial. The seed solution was then mixed by inversion for 2 minutes. After mixing, the solution turned light brown

with a pink tinge. The seed solution was allowed to sit at room temperature for 2 hours, during which time the growth solution was prepared. The growth solution consisted of 40 mL of 0.1 M CTAB solution, 2 mL of 0.01 M $HAuCl_4$ solution, 0.6 mL of 0.01 M silver nitrate solution, and 0.8 mL of 1 M hydrochloric acid in an Erlenmeyer flask with a ground-glass stopper. The growth solution was swirled briefly after each addition of silver nitrate and hydrochloric acid. Next, 0.32 mL of 0.1 M ascorbic acid was added to the growth solution. After swirling for ~30 seconds the solution turned completely clear. Finally, after the 2 hour waiting period, a 10% dilution of the seed solution was made with 18.2 Ωcm resistivity nanopure water. 100 uL of the 10% seed solution was added to the growth solution, after which the nanorod synthesis was allowed to come to completion overnight at room temperature. The nanorods were determined to have average dimensions of 65 ± 5 nm in length and 30 ± 4 nm in diameter determined from electron micrographs taken using a Hitachi S-5500 STEM, Figure 3.1.

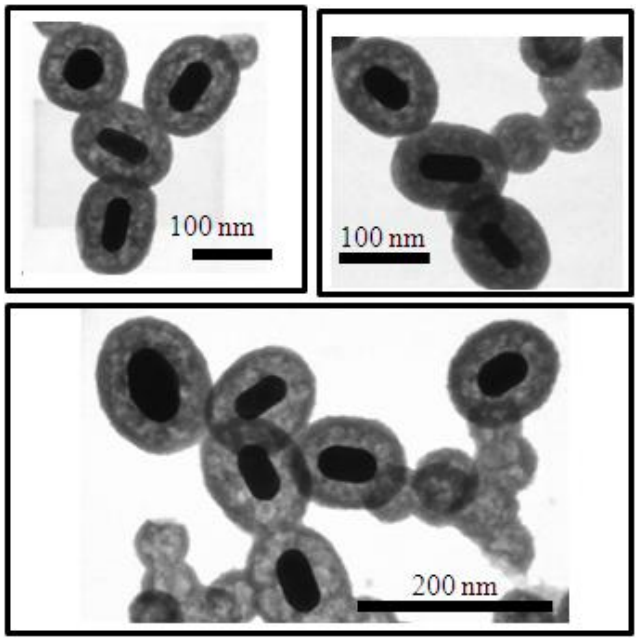

Figure 3.1: STEM micrographs of mesoporous silica coated nanorods.

3.2.2 Coating gold nanorods with dye-doped meoporous silica

The as-synthesized gold nanorods were coated with mesoporous silica based on the protocol outlined by Yan *et al.*[15]. First, 2 mL of the gold nanorods were centrifuged at 6,000 rpm for 10 minutes. The supernatant was decanted and the pellet was resuspended in 2 mL of nanopure water. This centrifugation step was repeated for one more cycle. Next, 20 μL of 1.4 mM R6G in methanol and 20 μL of 0.1 M sodium hydroxide aqueous solution were added and the solution was vortexed for several seconds. Three injections of 12 μL of 20 vol % of tetraethyl orthosilicate in methanol were added to the solution in 1 hour intervals while the solution was gently stirring on an orbital shaker. The solution was left to stir for 14 hours. The solution was then centrifuged at 8,000 rpm for 20 minutes, the supernatant was decanted and the pellets resuspended in 2 mL of methanol. This washing cycle was repeated once more. Finally, the solution was centrifuged again but this time resuspended in 2 mL of nanopure water. The R6G dye molecules are embedded into the silica shell during its formation. A molecule can become trapped into a pore as the silica forms around it and the ionic bond that will form should create a high affinity of the R6G to the silica. The mesoporous silica coating thickness was determined to be 34 ± 2 nm. The particles can be seen in Figure 3.1. The average length and width for the silica-coated particles shown in the three STEM micrographs were measured to be 132 ± 6 nm long and 97 ± 5 nm respectively.

3.2.3 Sample Preparation

25 x 25 mm #1 thickness cover slips were cleaned in an argon plasma for 15 minutes, coated with 1% aqueous polydiallyldimethylammonium chloride, and stirred on an orbital shaker for 10 minutes. The slide was then rinsed with nanopure water and dried under nitrogen. 45 μL of the above-described R6G doped mesoporous coated nanorod solution was dropped onto a cover slip for 5 minutes while stirring on an orbital shaker.

The slide was then thoroughly rinsed with nanopure water, to remove excess sample that has not adsorbed to the cover slip, and dried under nitrogen.

3.2.4 Microscopy

The experiments were carried out on an Olympus IX-71 inverted microscope with an Olympus 60x oil-immersion objective with N.A. of 1.45 (Figure 3.2). The fluorescence excitation of the R6G molecules was achieved with a quasi-circularly polarized 50 mW 532 nm laser (CrystaLaser). The excitation light is passed through the objective at the critical angle that is necessary for total internal reflection (TIR) excitation at the sample plane. This angle is set by passing the excitation light through a plano-convex lens that is mounted on a micrometer translation stage perpendicular to the incoming excitation light. The lens is placed in front of the back port of the microscope; therefore the excitation light passes through the TIR lens before entering the microscope.

The resulting fluorescence emission is collected by the same objective and then passed through a 532 nm dichroic (Semrock Di02-R532-25x36) and a long pass filter (Semrock LP03- 532RU) before imaging with a Princeton Instruments PhotonMax electron-multiplied CCD. The exposure time for fluorescence imaging was set at 10 ms. As previously discussed in chapter two, the actual integration time was 34.2 ms. This discrepancy in integration time was discovered after these initial experiments were completed; however, this has no effect on the data analysis. Nevertheless, it does mean that fluorescence emission was acquired for longer integration periods than expected which will lead to higher detected intensity and longer movies.

The microscope was also equipped for dark field scattering imaging with the use of an external halogen lamp. The white light is fiber coupled and is co-aligned with the laser excitation. The dark field scattering images were acquired for 0.3 s. A liquid crystal

tunable filter (LCTF), with the ability to selectively pass a specific wavelength, was placed in the path of the white light. To create local surface plasmon resonance (LSPR) spectra for the mesoporous silica coated nanorods the LCTF can be used to illuminate the sample with one specific wavelength at a time. The scattering emission at each wavelength, 450- 720 nm, is acquired for two accumulations at 0.5 s. The LSPR spectra are constructed by graphing the intensity of scattered light as a function of wavelength with the use of MATLAB code. The sample on the stage was covered with a home-built nitrogen flow chamber.

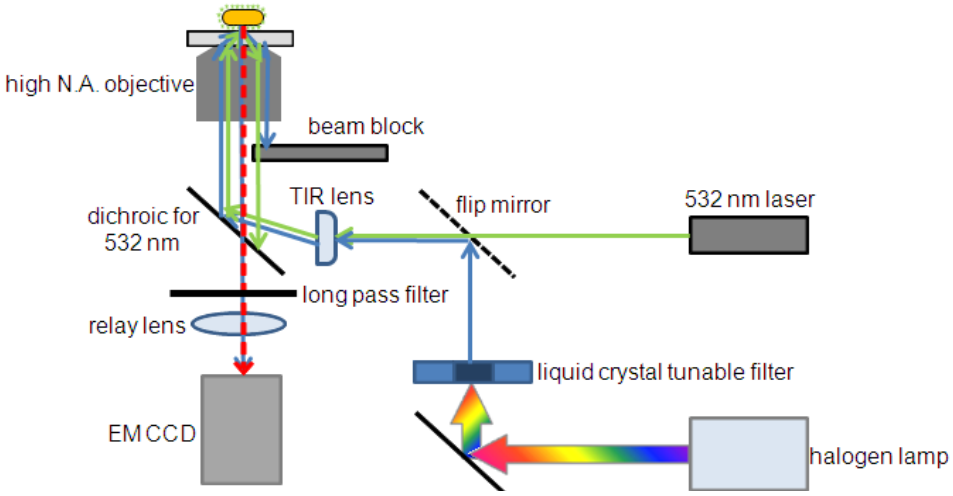

Figure 3.2: Schematic of the optical setup used to collect GSDIM fluorescence emission and dark field images for the nanorod-fluorophore system.

3.2.5 GSDIM data analysis

The raw data collected for these experiments are the same as the nanowire-fluorophore system, 1875 stacked tiff images of 512 x 512 pixels. All analysis was carried out using MATLAB code developed in-house. The procedure can be briefly described as follows: first, frames corresponding to fluorescent bursts are identified by looking for signals above a manually drawn threshold (Figure 3.3). The bursts above this

threshold occur when molecules are in the "on" state. The data points below the threshold occur when the molecule is in the "off" state. One might expect the signal to go down to zero if the molecules are truly in this "off" state and unable to fluoresce. However, this is not the case due to the inherent luminescence of the gold nanorod[52, 53]. This luminescence provides a constant background signal and will be apparent when no fluorescent bursts are occurring, *i.e.* when molecules are in the "off" state. The constant luminescence can be removed by subtracting successive frames, *e.g.* subtracting an "on" frame from a previous "off" frame[42, 51]. The nanorod luminescence signal, once distinguished from fluorescent bursts intensity, also acts as an alignment marker to account for mechanical drift during experimental data acquisition[35, 40, 51]. After each fluorescent burst is fit to equation one; the resultant fit was given a goodness of fit parameter between 0-1 depending on how well the emission point spread function was able to be fit to a Gaussian. The centroid positions with goodness of fit above 0.8 are used to create a scatter plots and spatial histograms, as described in Chapter two.

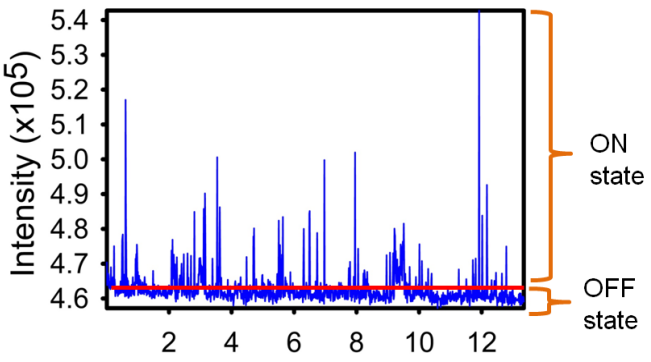

Figure 3.3: Integrated intensity time trace showing fluorescence bursts associated with GSDIM. The red line is an example of a manually drawn threshold to separate fluorescent "on" frames from non-fluorescent "off" frames.

3.3 RESULTS AND DISCUSSION

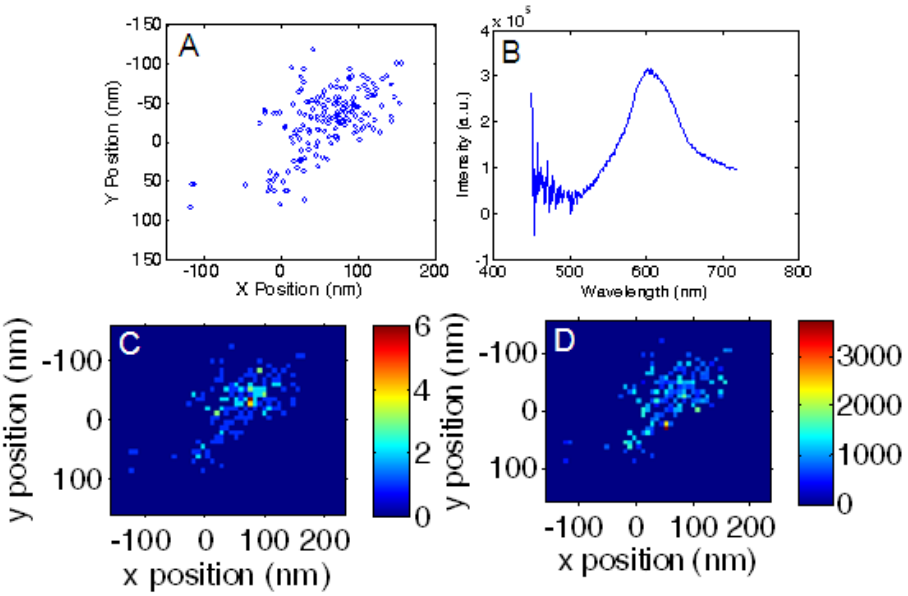

Figure 3.4: (A) Scatter plot showing the values of (x_0, y_0) for the Gaussian centroid fits to each fluorescence burst. (B) The LSPR spectrum of the nanorod coated by the mesoporous silica. (C) Spatial frequency histogram showing the number of bursts observed at a particular location in the mesoporous silica shell around the nanorod. Bin size is 7.7 nm. (D) Spatial intensity histogram showing the average intensity of fluorescent bursts in a particular bin. Bin size is 7.7 nm.

Figure 3.4 shows an example of using GSDIM to reconstruct the size and shape of a mesoporous silica coated gold nanorod. The results are from two movies, each with 1,875 frames. As previously described in the GSDIM data analysis section, the centroid positions of all the GSDIM bursts are plotted in a scatter plot (Figure 3.4A). The scatter plot shows a rod-like shape, however, several sporadic bursts were localized away from the bulk of the centroid positions. These sporadic bursts could be caused by emission from R6G molecules that were deposited on the cover slip along with the mesoporous silica coated nanorods. This is not very likely due to the three cycles of centrifugation

rinsing done on the sample before it is deposited on the cover slip. The extra rinsing should eliminate free R6G molecules in solution. Furthermore, this is unlikely because R6G forms a strong ionic bond with the silica coating. Therefore, R6G molecules in solution should be bound to the silica. A more reasonable cause for the seemingly sporadic localization is that only a fraction of the molecules in the mesoporous silica shell are being sampled. This idea is more reasonable because the centroid positions shown in the scatter plot should be centered on the point (0, 0). This point corresponds to the nanorod's inherent luminescence signal converged to a signal spot. The luminescence point should be localized in the middle of all the localized GSDIM fluorescence bursts. Unfortunately, this is not the case. The data in Figure 3.4 suggests that only half of the silica coated nanorod is being reconstructed due to the limited detection of GSDIM signal from all the molecules in the entire silica shell, thus creating an incomplete image. This incomplete picture is likely due to the steric hindrances caused by a fluorophore being trapped in a pore. The hindrance can inhibit conformational flexibility, which can effectively inhibit fluorescence emission because the molecule will not be able to properly align itself with the excitation polarization of the laser.

To further analyze this data a frequency spatial histogram (Figure 3.4C) was created. The histogram depicts the centroid points in the scatter plot binned in 7.7 nm squares; the color key next to the histogram shows the frequency of GSDIM bursts that occurred in a specific bin. The histogram shows evenly distributed frequency over the reconstructed image. The intensity histogram, Figure 3.4D, shows the average fluorescence intensity in a particular bin. The intensity of GSDIM bursts is also evenly distributed. The fact that intensities of orders of magnitude higher than the actual results shown in Figure 3.4D were not observed provides evidence that surface enhanced fluorescence is not occurring.[75, 84] The GSDIM information acquired is, therefore, only

representative of the available fluorophores that were probed in the amount of time given for data acquisition.

It should also be noted that the bulk of the centroid positions shown in Figure 3.4 occur approximately within a 172 nm long and 102 nm in wide rectangle. The width of this data agrees closely with the expected width of the mesoporous silica coated nanorod determined by STEM micrographs to be 97 ± 5 nm. However, the length is substantially longer than the expected value of 132 ± 6 nm. It could be hypothesized that the reconstructed image is actually two nanoparticles stacked end to end. However, this hypothesis can be negated due to the fact that the measured length is not long enough to indicate the presence of two nanorods. Moreover, the LSPR spectrum for the nanorod in this example, Figure 3.4B, is indicative of a single nanorod with a plasmon resonance peak of ~ 600 nm. This inaccuracy could be caused by plasmonic interactions between the nanorod and the emitting fluorophore[42]. If the fluorophore's emission were to couple into the plasmon modes of the nanorod then it would be reradiated back into free space at a distorted angle, which will affect the collected emission.[91] When this distorted emission is collected back through the objective to be detected, its localized position would not be representative of its actual position of the R6G in the mesoporous silica shell. This inconsistency remains a reoccurring problem that is also observed in Figures 3.5 and 3.6.

Figure 3.5 depicts another example of a reconstructed mesoporous silica-coated nanorod, orientated differently than the particle shown in Figure 3.4. A nanorod-like shape is reconstructed; however the same issues with localized sporadic bursts can be observed, as previously discussed with Figure 3.4. The frequency and intensity spatial histograms (Figures 3.5C and 3.5D respectively) show evenly distributed amounts of fluorescent bursts and intensity. The bulk of the fluorescent bursts in this figure occur within a 190 x 86 nm rectangle. The width, 86 nm, corresponds well with the expected

width of these mesoporous silica coated nanorods. The length, once again, is longer than expected. Figure 3.5 also provides another example where the location of the converged nanorod luminescence is not centered with respect to the localized fluorescent bursts.

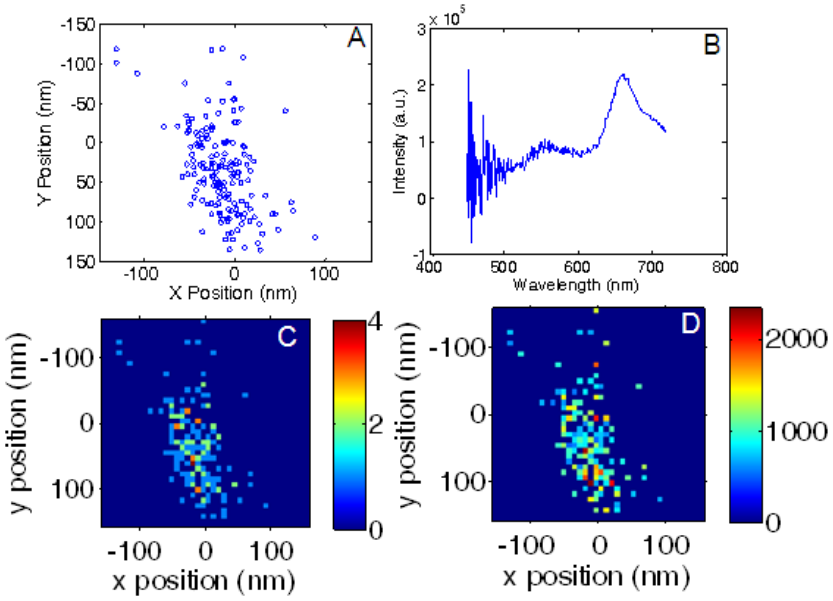

Figure 3.5: (A) Scatter plot showing the values of (x_0, y_0) for the Gaussian centroid fits to each fluorescence burst. (B) The LSPR spectrum of the nanorod coated by the mesoporous silica. (C) Spatial frequency histogram showing the number of bursts observed at a particular location in the mesoporous silica shell around the nanorod. Bin size is 7.7 nm. (D) Spatial intensity map showing the average intensity of fluorescent bursts in a particular bin. Bin size is 7.7 nm.

The LSPR spectrum for this nanorod, Figure 3.5B, provides evidence that another particle with an LSPR of ~550 nm was present in this example. The LSPR peak of ~550 nm suggests that the particle is most likely a nanosphere[92]. The silica coated nanosphere could also be contributing to this appreciably longer measured length. Unfortunately, because typically only a small fraction of fluorophores in the mesoporous

silica shells are being sampled it is difficult to differentiate between multiple nanoparticles that could be in the reconstructed images.

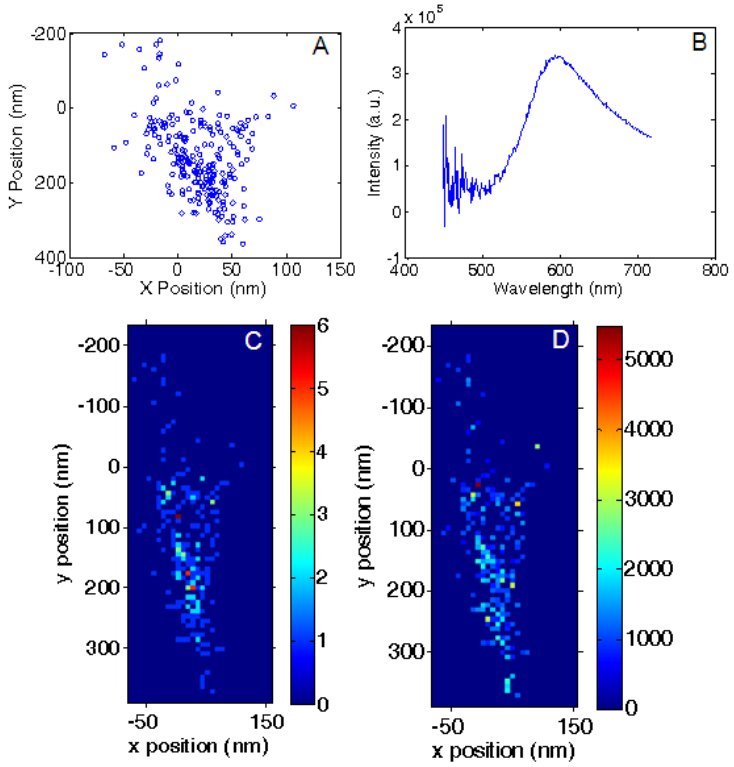

Figure 3.6: (A) Scatter plot showing the values of (x_0, y_0) for the Gaussian centroid fits to each fluorescence burst. (B) The LSPR spectrum of the nanorod coated by the mesoporous silica. (C) Spatial frequency histogram showing the number of bursts observed at a particular location in the mesoporous silica shell around the nanorod. Bin size is 7.7 nm. (D) Spatial intensity map showing the average intensity of fluorescent bursts in a particular bin. Bin size is 7.7 nm.

Figure 3.6 provides an example for utilizing GSDIM to reconstruct a nanorod aggregate, possibly a dimer with nanorods stacked closely in an end to end fashion. The broad LSPR peak in figure 3.6B is indicative of more than one linearly aligned nanorod[93, 94]. Although this example portrays a possible dimer, it is still expected that the nanorod

luminescence should converge in the middle of the centroid positions for all the fluorescent bursts. Again, we observe minimal number of fluorescent centroid points located to the upper right of (0, 0).

Two possible origins for this reoccurring discrepancy can be hypothesized: first, sampling from only a small fraction of the R6G molecules embedded into the silica shell can yield these incomplete reconstructed images. A second hypothesis is plasmon-directed fluorescence emission, which was just discussed.[51]

One might expect there to be a field of high electromagnetic enhancement in the junction region between the nanoparticles creating a hot spot region for surface enhanced fluorescence.[84, 95] The intensity spatial histogram (Figure 3.6D) does not support this data possibly due to the fact that the nanorods are individually coated with silica. The silica thickness can inhibit the creation of such a hot spot, due to the distance it creates between the nanorods.

3.4 CONCLUSION

GSDIM is capable of providing sub-diffraction limited characterization of mesoporous silica coated nanorods. Unfortunately, two occurring issues made it difficult to definitively state that the correct dimensions of the nanorods were being reconstructed. The gold nanorod luminescence signal in each of the examples did not converge to the center of all the fluorescent burst centroids. Also, the GSDIM data that was reconstructed yielded results in the length dimension that were substantially longer than expected for single coated nanorods. In order to further probe these reoccurring issues, changing the optical setup used for the experiment may be necessary. The TIR geometry may be introducing unwanted difficulties; instead epi-illumination geometry may be more beneficial and simple. Also, generating new MATLAB code that is better suited for

modeling a fluorophores emission near a metal surface would be beneficial. Solving these problems may yield more reliable reconstructed images with the expected size dimensions.

3.5 ACKNOWLEDGEMENTS

I gratefully acknowledge Kathryn M. Mayer and Maggie L. Weber for assisting me in the work shown in this chapter. I also acknowledge the NSF IGERT "Atomic and Molecular Imaging" Program (grant no. DGE-0549417) for fellowship support. I would also like to thank the National Science Foundation (Grant No. 0821312) for funding the Hitachi S-5500 scanning electron microscope/scanning transmission electron microscope used in this work and Texas Materials Institute for supporting this facility. This material is based on work supported by the Welch Foundation under Award No. F-1699.

References

1. Huang, X.; El-Sayed, I. H.; Qian, W.; El-Sayed, M. A., Cancer Cell Imaging and Photothermal Therapy in the Near-Infrared Region by Using Gold Nanorods. *J. Am. Chem. Soc.* **2006,** 128, (6), 2115-2120.
2. Ando, J.; Fujita, K.; Smith, N. I.; Kawata, S., Dynamic SERS Imaging of Cellular Transport Pathways with Endocytosed Gold Nanoparticles. *Nano Lett.* **2011,** 11, (12), 5344-5348.
3. Gu, Y.; Sun, W.; Wang, G.; Fang, N., Single Particle Orientation and Rotation Tracking Discloses Distinctive Rotational Dynamics of Drug Delivery Vectors on Live Cell Membranes. *J. Am. Chem. Soc.* **2011,** 133, (15), 5720-5723.
4. Boisselier, E.; Astruc, D., Gold nanoparticles in nanomedicine: preparations, imaging, diagnostics, therapies and toxicity. *Chem. Soc. Rev.* **2009,** 38, (6), 1759-1782.
5. Song, J.; Zhou, J.; Duan, H., Self-Assembled Plasmonic Vesicles of SERS-Encoded Amphiphilic Gold Nanoparticles for Cancer Cell Targeting and Traceable Intracellular Drug Delivery. *J. Am. Chem. Soc.* **2012,** 134, (32), 13458-13469.
6. Yang, X.; Liu, X.; Liu, Z.; Pu, F.; Ren, J.; Qu, X., Near-Infrared Light-Triggered, Targeted Drug Delivery to Cancer Cells by Aptamer Gated Nanovehicles. *Adv. Mater. (Weinheim, Ger.)* **2012,** 24, (21), 2890-2895.
7. de, l. R. R.; Aili, D.; Stevens, M. M., Enzyme-responsive nanoparticles for drug release and diagnostics. *Adv. Drug Delivery Rev.* **2012,** 64, (11), 967-978.
8. Hirsch, L. R.; Stafford, R. J.; Bankson, J. A.; Sershen, S. R.; Rivera, B.; Price, R. E.; Hazle, J. D.; Halas, N. J.; West, J. L., Nanoshell-mediated near-infrared thermal therapy of tumors under magnetic resonance guidance. *Proc. Natl. Acad. Sci. U. S. A.* **2003,** 100, (23), 13549-13554.
9. Wang, J.; Zhu, G.; You, M.; Song, E.; Shukoor, M. I.; Zhang, K.; Altman, M. B.; Chen, Y.; Zhu, Z.; Huang, C. Z.; Tan, W., Assembly of Aptamer Switch Probes and Photosensitizer on Gold Nanorods for Targeted Photothermal and Photodynamic Cancer Therapy. *ACS Nano* **2012,** 6, (6), 5070-5077.
10. De, M.; Ghosh, P. S.; Rotello, V. M., Applications of nanoparticles in biology. *Adv. Mater. (Weinheim, Ger.)* **2008,** 20, (22), 4225-4241.
11. Guerrero-Martinez, A.; Perez-Juste, J.; Liz-Marzan, L. M., Recent Progress on Silica Coating of Nanoparticles and Related Nanomaterials. *Adv. Mater. (Weinheim, Ger.)* **2010,** 22, (11), 1182-1195.
12. Wang, Z.; Zong, S.; Yang, J.; Li, J.; Cui, Y., Dual-mode probe based on mesoporous silica coated gold nanorods for targeting cancer cells. *Biosens. Bioelectron.* **2011,** 26, (6), 2883-2889.
13. Liu, S.; Han, M., Synthesis, functionalization, and bioconjugation of monodisperse, silica-coated gold nanoparticles: Robust bioprobes. *Adv. Funct. Mater.* **2005,** 15, (6), 961-967.
14. Wang, C.; Ma, Z.; Wang, T.; Su, Z., Synthesis, assembly, and biofunctionalization of silica-coated gold nanorods for colorimetric biosensing. *Adv. Funct. Mater.* **2006,** 16, (13), 1673-1678.

15. Ming, T.; Zhao, L.; Yang, Z.; Chen, H.; Sun, L.; Wang, J.; Yan, C., Strong Polarization Dependence of Plasmon-Enhanced Fluorescence on Single Gold Nanorods. *Nano Lett.* **2009,** 9, (11), 3896-3903.
16. Sperling, R. A.; Rivera, G. P.; Zhang, F.; Zanella, M.; Parak, W. J., Biological applications of gold nanoparticles. *Chem. Soc. Rev.* **2008,** 37, (9), 1896-1908.
17. Zhang, J.; Lakowicz, J. R., A Model for DNA Detection by Metal-Enhanced Fluorescence from Immobilized Silver Nanoparticles on Solid Substrate. *J. Phys. Chem. B* **2006,** 110, (5), 2387-2392.
18. Maxwell, D. J.; Taylor, J. R.; Nie, S., Self-assembled nanoparticle probes for recognition and detection of biomolecules. *J. Am. Chem. Soc.* **2002,** 124, (32), 9606-9612.
19. Rust, M. J.; Bates, M.; Zhuang, X., Sub-diffraction-limit imaging by stochastic optical reconstruction microscopy (STORM). *Nat. Methods* **2006,** 3, (10), 793-796.
20. Thompson, R. E.; Larson, D. R.; Webb, W. W., Precise nanometer localization analysis for individual fluorescent probes. *Biophys. J.* **2002,** 82, (5), 2775-2783.
21. Gordon, M. P.; Ha, T.; Selvin, P. R., Single-molecule high-resolution imaging with photobleaching. *Proc. Natl. Acad. Sci. U. S. A.* **2004,** 101, (17), 6462-6465.
22. Qu, X.; Wu, D.; Mets, L.; Scherer, N. F., Nanometer-localized multiple single-molecule fluorescence microscopy. *Proc. Natl. Acad. Sci. U. S. A.* **2004,** 101, (31), 11298-11303.
23. Betzig, E.; Patterson, G. H.; Sougrat, R.; Lindwasser, O. W.; Olenych, S.; Bonifacino, J. S.; Davidson, M. W.; Lippincott-Schwartz, J.; Hess, H. F., Imaging Intracellular Fluorescent Proteins at Nanometer Resolution. *Science (Washington, DC, U. S.)* **2006,** 313, (5793), 1642-1645.
24. Folling, J.; Bossi, M.; Bock, H.; Medda, R.; Wurm, C. A.; Hein, B.; Jakobs, S.; Eggeling, C.; Hell, S. W., Fluorescence nanoscopy by ground-state depletion and single-molecule return. *Nat Methods* **2008,** 5, (11), 943-5.
25. Moerner, W. E., Microscopy beyond the diffraction limit using actively controlled single molecules. *J Microsc* **2012,** 246, (3), 213-20.
26. Steinhauer, C.; Forthmann, C.; Vogelsang, J.; Tinnefeld, P., Superresolution Microscopy on the Basis of Engineered Dark States. *J. Am. Chem. Soc.* **2008,** 130, (50), 16840-16841.
27. van, d. L. S.; Kasper, R.; Heilemann, M.; Sauer, M., Photoswitching microscopy with standard fluorophores. *Appl. Phys. B: Lasers Opt.* **2008,** 93, (4), 725-731.
28. Xu, K.; Babcock, H. P.; Zhuang, X., Dual-objective STORM reveals three-dimensional filament organization in the actin cytoskeleton. *Nat. Methods* **2012,** 9, (2), 185-188.
29. Lippincott-Schwartz, J.; Manley, S., Putting super-resolution fluorescence microscopy to work. *Nat. Methods* **2009,** 6, (1), 21-23.
30. Shroff, H.; Galbraith, C. G.; Galbraith, J. A.; White, H.; Gillette, J.; Olenych, S.; Davidson, M. W.; Betzig, E., Dual-color superresolution imaging of genetically expressed probes within individual adhesion complexes. *Proc. Natl. Acad. Sci. U. S. A.* **2007,** 104, (51), 20308-20313.

31. Fernandez-Suarez, M.; Ting, A. Y., Fluorescent probes for super-resolution imaging in living cells. *Nat. Rev. Mol. Cell Biol.* **2008,** 9, (12), 929-943.
32. Huang, B.; Bates, M.; Zhuang, X., Super-resolution fluorescence microscopy. *Annu. Rev. Biochem.* **2009,** 78, 993-1016.
33. Gould, T. J.; Gunewardene, M. S.; Gudheti, M. V.; Verkhusha, V. V.; Yin, S.-R.; Gosse, J. A.; Hess, S. T., Nanoscale imaging of molecular positions and anisotropies. *Nat. Methods* **2008,** 5, (12), 1027-1030.
34. Huang, B.; Babcock, H.; Zhuang, X.-W., Breaking the Diffraction Barrier: Super-Resolution Imaging of Cells. *Cell (Cambridge, MA, U. S.)* **2010,** 143, (7), 1047-1058.
35. Stranahan, S. M.; Willets, K. A., Super-resolution Optical Imaging of Single-Molecule SERS Hot Spots. *Nano Lett.* **2010,** 10, (9), 3777-3784.
36. Weber, M. L.; Litz, J. P.; Masiello, D. J.; Willets, K. A., Super-Resolution Imaging Reveals a Difference between SERS and Luminescence Centroids. *ACS Nano* **2012,** 6, (2), 1839-1848.
37. Weber, M. L.; Willets, K. A., Correlated Super-Resolution Optical and Structural Studies of Surface-Enhanced Raman Scattering Hot Spots in Silver Colloid Aggregates. *J. Phys. Chem. Lett.* **2011,** 2, (14), 1766-1770.
38. Titus, E. J.; Weber, M. L.; Stranahan, S. M.; Willets, K. A., Super-Resolution SERS Imaging beyond the Single-Molecule Limit: An Isotope-Edited Approach. *Nano Lett.* **2012,** 12, (10), 5103-5110.
39. Cang, H.; Labno, A.; Lu, C.; Yin, X.; Liu, M.; Gladden, C.; Liu, Y.; Zhang, X., Probing the electromagnetic field of a 15-nanometer hotspot by single molecule imaging. *Nature (London, U. K.)* **2011,** 469, (7330), 385-388.
40. Zhou, X.; Andoy, N. M.; Liu, G.; Choudhary, E.; Han, K.-S.; Shen, H.; Chen, P., Quantitative super-resolution imaging uncovers reactivity patterns on single nanocatalysts. *Nat. Nanotechnol.* **2012,** 7, (4), 237-241.
41. Davies, M.; Wochnik, A.; Feil, F.; Jung, C.; Braeuchle, C.; Scheu, C.; Michaelis, J., Synchronous Emission from Nanometric Silver Particles through Plasmonic Coupling on Silver Nanowires. *ACS Nano* **2012,** 6, (7), 6049-6057.
42. Lin, H.; Centeno, S. P.; Su, L.; Kenens, B.; Rocha, S.; Sliwa, M.; Hofkens, J.; Uji-i, H., Mapping of Surface-Enhanced Fluorescence on Metal Nanoparticles using Super-Resolution Photoactivation Localization Microscopy. *ChemPhysChem* **2012,** 13, (4), 973-981.
43. Vamosi, G.; Gohike, C.; Clegg, R. M., Fluorescence characteristics of 5-carboxytetramethylrhodamine linked covalently to the 5' end of oligonucleotides: multiple conformers of single-stranded and double-stranded dye-DNA complexes. *Biophys. J.* **1996,** 71, (2), 972-994.
44. Neubrech, F.; Pucci, A.; Cornelius, T. W.; Karim, S.; Garcia-Etxarri, A.; Aizpurua, J., Resonant Plasmonic and Vibrational Coupling in a Tailored Nanoantenna for Infrared Detection. *Phys. Rev. Lett.* **2008,** 101, (15), 157403/1-157403/4.
45. Wei, H.; Ratchford, D.; Li, X.; Xu, H.; Shih, C.-K., Propagating Surface Plasmon Induced Photon Emission from Quantum Dots. *Nano Lett.* **2009,** 9, (12), 4168-4171.

46. Taminiau, T. H.; Stefani, F. D.; Segerink, F. B.; Van, H. N. F., Optical antennas direct single-molecule emission. *Nat. Photonics* **2008,** 2, (4), 234-237.
47. Frimmer, M.; Chen, Y.; Koenderink, A. F., Scanning Emitter Lifetime Imaging Microscopy for Spontaneous Emission Control. *Phys. Rev. Lett.* **2011,** 107, (12), 123602/1-123602/5.
48. Kim, F.; Sohn, K.; Wu, J.; Huang, J., Chemical Synthesis of Gold Nanowires in Acidic Solutions. *J. Am. Chem. Soc.* **2008,** 130, (44), 14442-14443.
49. Jones, M. R.; MacFarlane, R. J.; Lee, B.; Zhang, J.; Young, K. L.; Senesi, A. J.; Mirkin, C. A., DNA-nanoparticle superlattices formed from anisotropic building blocks. *Nat. Mater.* **2010,** 9, (11), 913-917.
50. Integrated DNA Technologies, I. Modifications/Dyes https://www.idtdna.com/catalog/Modifications/Dyes.aspx (November 26, 2012),
51. Blythe, K. L.; Mayer, K. M.; Weber, M. L.; Willets, K. A., Ground state depletion microscopy for imaging interactions between gold nanowires and fluorophore-labeled ligands. *Phys Chem Chem Phys* **2012**.
52. Link, S.; El-Sayed, M. A., Shape and size dependence of radiative, non-radiative and photothermal properties of gold nanocrystals. *Int. Rev. Phys. Chem.* **2000,** 19, (3), 409-453.
53. Mohamed, M. B.; Volkov, V.; Link, S.; El-Sayed, M. A., The 'lightning' gold nanorods: fluorescence enhancement of over a million compared to the gold metal. *Chem. Phys. Lett.* **2000,** 317, (6), 517-523.
54. Stoermer, R. L.; Keating, C. D., Distance-Dependent Emission from Dye-Labeled Oligonucleotides on Striped Au/Ag Nanowires: Effect of Secondary Structure and Hybridization Efficiency. *J. Am. Chem. Soc.* **2006,** 128, (40), 13243-13254.
55. Kim, H.; Xiang, C.; Guell, A. G.; Penner, R. M.; Potma, E. O., Tunable Two-Photon Excited Luminescence in Single Gold Nanowires Fabricated by Lithographically Patterned Nanowire Electrodeposition. *J. Phys. Chem. C* **2008,** 112, (33), 12721-12727.
56. Geddes, C. D.; Parfenov, A.; Gryczynski, I.; Lakowicz, J. R., Luminescent blinking of gold nanoparticles. *Chem. Phys. Lett.* **2003,** 380, (3,4), 269-272.
57. van, D. M. A.; Lippitz, M.; Orrit, M., Far-Field Optical Microscopy of Single Metal Nanoparticles. *Acc. Chem. Res.* **2005,** 38, (7), 594-601.
58. Geddes, C. D.; Gryczynski, I.; Parfenov, A.; Aslan, K.; Lakowicz, J. R., Luminescent blinking from silver, gold and copper nanostructures: a new class of probes for imaging and localization. *Proc. SPIE-Int. Soc. Opt. Eng.* **2004,** 5329, (Genetically Engineered and Optical Probes for Biomedical Applications II), 276-286.
59. Yuan, C. T.; Chou, W. C.; Tang, J.; Lin, C. A.; Chang, W. H.; Shen, J. L.; Chuu, D. S., Single fluorescent gold nanoclusters. *Opt. Express* **2009,** 17, (18), 16111-16118.
60. Hill, H. D.; Millstone, J. E.; Banholzer, M. J.; Mirkin, C. A., The Role Radius of Curvature Plays in Thiolated Oligonucleotide Loading on Gold Nanoparticles. *ACS Nano* **2009,** 3, (2), 418-424.
61. Caswell, K. K.; Wilson, J. N.; Bunz, U. H. F.; Murphy, C. J., Preferential end-to-end assembly of gold nanorods by biotin-streptavidin connectors. *J. Am. Chem. Soc.* **2003,** 125, (46), 13914-13915.

62. Chang, J.-Y.; Wu, H.; Chen, H.; Ling, Y.-C.; Tan, W., Oriented assembly of Au nanorods using biorecognition system. *Chem. Commun. (Cambridge, U. K.)* **2005**, (8), 1092-1094.
63. Hwang, S.-Y.; Tao, A. R., Biofunctionalization of gold nanorods. *Pure Appl. Chem.* **2012,** 83, (1), 233-241.
64. Nikoobakht, B.; El-Sayed, M. A., Evidence for Bilayer Assembly of Cationic Surfactants on the Surface of Gold Nanorods. *Langmuir* **2001,** 17, (20), 6368-6374.
65. Johnson, C. J.; Dujardin, E.; Davis, S. A.; Murphy, C. J.; Mann, S., Growth and form of gold nanorods prepared by seed-mediated, surfactant-directed synthesis. *J. Mater. Chem.* **2002,** 12, (6), 1765-1770.
66. Gao, J.; Bender, C. M.; Murphy, C. J., Dependence of the Gold Nanorod Aspect Ratio on the Nature of the Directing Surfactant in Aqueous Solution. *Langmuir* **2003,** 19, (21), 9065-9070.
67. Shegai, T.; Huang, Y.; Xu, H.; Kaell, M., Coloring fluorescence emission with silver nanowires. *Appl. Phys. Lett.* **2010,** 96, (10), 103114/1-103114/3.
68. Chen, Y.; Nielsen, T. R.; Gregersen, N.; Lodahl, P.; Mork, J., Finite-element modeling of spontaneous emission of a quantum emitter at nanoscale proximity to plasmonic waveguides. *Phys. Rev. B: Condens. Matter Mater. Phys.* **2010,** 81, (12), 125431/1-125431/11.
69. Fedutik, Y.; Temnov, V.; Woggon, U.; Ustinovich, E.; Artemyev, M., Exciton-Plasmon Interaction in a Composite Metal-Insulator-Semiconductor Nanowire System. *J. Am. Chem. Soc.* **2007,** 129, (48), 14939-14945.
70. Chang, D. E.; Soerensen, A. S.; Hemmer, P. R.; Lukin, M. D., Strong coupling of single emitters to surface plasmons. *Phys. Rev. B: Condens. Matter Mater. Phys.* **2007,** 76, (3), 035420/1-035420/26.
71. Gramotnev, D. K.; Bozhevolnyi, S. I., Plasmonics beyond the diffraction limit. *Nat. Photonics* **2010,** 4, (2), 83-91.
72. Pyayt, A. L.; Wiley, B.; Xia, Y.; Chen, A.; Dalton, L., Integration of photonic and silver nanowire plasmonic waveguides. *Nat. Nanotechnol.* **2008,** 3, (11), 660-665.
73. Han, K. Y.; Kim, S. K.; Eggeling, C.; Hell, S. W., Metastable Dark States Enable Ground State Depletion Microscopy of Nitrogen Vacancy Centers in Diamond with Diffraction-Unlimited Resolution. *Nano Lett.* **2010,** 10, (8), 3199-3203.
74. Rittweger, E.; Wildanger, D.; Hell, S. W., Far-field fluorescence nanoscopy of diamond color centers by ground state depletion. *EPL* **2009,** 86, (1), 14001/1-14001/6.
75. Fu, Y.; Zhang, J.; Lakowicz, J. R., Plasmon-Enhanced Fluorescence from Single Fluorophores End-Linked to Gold Nanorods. *J. Am. Chem. Soc.* **2010,** 132, (16), 5540-5541.
76. Huschka, R.; Zuloaga, J.; Knight, M. W.; Brown, L. V.; Nordlander, P.; Halas, N. J., Light-Induced Release of DNA from Gold Nanoparticles: Nanoshells and Nanorods. *J. Am. Chem. Soc.* **2011,** 133, (31), 12247-12255.
77. Knight, M. W.; Grady, N. K.; Bardhan, R.; Hao, F.; Nordlander, P.; Halas, N. J., Nanoparticle-Mediated Coupling of Light into a Nanowire. *Nano Lett.* **2007,** 7, (8), 2346-2350.

78. Wustholz, K. L.; Henry, A.-I.; McMahon, J. M.; Freeman, R. G.; Valley, N.; Piotti, M. E.; Natan, M. J.; Schatz, G. C.; Van, D. R. P., Structure-Activity Relationships in Gold Nanoparticle Dimers and Trimers for Surface-Enhanced Raman Spectroscopy. *J. Am. Chem. Soc.* **2010,** 132, (31), 10903-10910.
79. McMahon, J. M.; Henry, A.-I.; Wustholz, K. L.; Natan, M. J.; Freeman, R. G.; Van, D. R. P.; Schatz, G. C., Gold nanoparticle dimer plasmonics: finite element method calculations of the electromagnetic enhancement to surface-enhanced Raman spectroscopy. *Anal. Bioanal. Chem.* **2009,** 394, (7), 1819-1825.
80. Kim, K.; Shin, D.; Kim, K. L.; Shin, K. S., Electromagnetic field enhancement in the gap between two Au nanoparticles: the size of hot site probed by surface-enhanced Raman scattering. *Phys Chem Chem Phys* **2010,** 12, (15), 3747-52.
81. Aizenberg, J.; Black, A. J.; Whitesides, G. M., Controlling local disorder in self-assembled monolayers by patterning the topography of their metallic supports. *Nature (London)* **1998,** 394, (6696), 868-871.
82. Wei, H.; Hao, F.; Huang, Y.; Wang, W.; Nordlander, P.; Xu, H., Polarization Dependence of Surface-Enhanced Raman Scattering in Gold Nanoparticle-Nanowire Systems. *Nano Lett.* **2008,** 8, (8), 2497-2502.
83. Hao, F.; Nordlander, P., Plasmonic coupling between a metallic nanosphere and a thin metallic wire. *Appl. Phys. Lett.* **2006,** 89, (10), 103101/1-103101/3.
84. Fort, E.; Gresillon, S., Surface enhanced fluorescence. *J. Phys. D: Appl. Phys.* **2008,** 41, (1), 013001/1-013001/31.
85. Tran, M. L.; Centeno, S. P.; Hutchison, J. A.; Engelkamp, H.; Liang, D.; Van, T. G.; Sels, B. F.; Hofkens, J.; Uji-i, H., Control of Surface Plasmon Localization via Self-Assembly of Silver Nanoparticles along Silver Nanowires. *J. Am. Chem. Soc.* **2008,** 130, (51), 17240-17241.
86. Solis, D.; Chang, W.-S.; Khanal, B. P.; Bao, K.; Nordlander, P.; Zubarev, E. R.; Link, S., Bleach-Imaged Plasmon Propagation (BlIPP) in Single Gold Nanowires. *Nano Lett.* **2010,** 10, (9), 3482-3485.
87. Dempster, D. N.; Morrow, T.; Quinn, M. F., Photochemical characteristics of Rhodamine 6G-ethanol solutions. *J. Photochem.* **1974,** 2, (5), 343-59.
88. Nie, S.; Chiu, D. T.; Zare, R. N., Probing individual molecules with confocal fluorescence microscopy. *Science (Washington, D. C.)* **1994,** 266, (5187), 1018-21.
89. Liao, H.; Hafner, J. H., Gold Nanorod Bioconjugates. *Chem. Mater.* **2005,** 17, (18), 4636-4641.
90. Mayer, K. M.; Lee, S.; Liao, H.; Rostro, B. C.; Fuentes, A.; Scully, P. T.; Nehl, C. L.; Hafner, J. H., A Label-Free Immunoassay Based Upon Localized Surface Plasmon Resonance of Gold Nanorods. *ACS Nano* **2008,** 2, (4), 687-692.
91. Kuhn, S.; Hakanson, U.; Rogobete, L.; Sandoghdar, V., Enhancement of Single-Molecule Fluorescence Using a Gold Nanoparticle as an Optical Nanoantenna. *Phys. Rev. Lett.* **2006,** 97, (1), 017402/1-017402/4.
92. Jain, P. K.; Lee, K. S.; El-Sayed, I. H.; El-Sayed, M. A., Calculated Absorption and Scattering Properties of Gold Nanoparticles of Different Size, Shape, and

Composition: Applications in Biological Imaging and Biomedicine. *J. Phys. Chem. B* **2006,** 110, (14), 7238-7248.
93. Jain, P. K.; El-Sayed, M. A., Plasmonic coupling in noble metal nanostructures. *Chem. Phys. Lett.* **2010,** 487, (4-6), 153-164.
94. Thomas, K. G.; Barazzouk, S.; Ipe, B. I.; Joseph, S. T. S.; Kamat, P. V., Uniaxial Plasmon Coupling through Longitudinal Self-Assembly of Gold Nanorods. *J. Phys. Chem. B* **2004,** 108, (35), 13066-13068.
95. Nikoobakht, B.; El-Sayed, M. A., Surface-Enhanced Raman Scattering Studies on Aggregated Gold Nanorods. *J. Phys. Chem. A* **2003,** 107, (18), 3372-3378.